In utero gene transfer system for embryos before neural tube closure reveals a role for Hmga2 in the onset of neurogenesis

Naohiro Kuwayama[1], Yusuke Kishi[1,*], Yurie Maeda[1], Yurie Nishiumi[1], Yutaka Suzuki[2], Haruhiko Koseki[3], Yusuke Hirabayashi[4], and Yukiko Gotoh[1,5]

[1]Graduate School of Pharmaceutical Sciences, The University of Tokyo, Tokyo 113-0033, Japan
[2]Department of Computational Biology, Graduate School of Frontier Sciences, The University of Tokyo, Tokyo 277-8561, Japan
[3]Laboratory for Developmental Genetics, RIKEN Center for Integrative Medical Sciences (RIKEN-IMS), Tsurumi-ku, Yokohama 230-0045, Japan
[4]Graduate School of Engineering, The University of Tokyo, Tokyo 113-0033, Japan
[5]International Research Center for Neurointelligence (WPI-IRCN), The University of Tokyo, Tokyo 113-0033, Japan

*Correspondence: ykisi@mol.f.u-tokyo.ac.jp

Abstract

During the early stage of mammalian neural development, neuroepithelial cells (NECs) proliferate and increase their pool size before switching their fate to become neurogenic radial glial progenitors (RGPs). The timing of this expansion-to-neurogenic phase transition is strictly regulated so as to determine the proper number of progenitors and differentiated cell types that constitute the brain. The molecular mechanism underlying this switch has remained poorly understood, however, in part because of the difficulty associated with manipulation of gene expression in NECs before their transition to RGPs, which occurs before neural tube closure. We have now developed a simple and efficient method to manipulate gene expression in mouse neocortical NECs in the expansion phase by in utero injection of viral vectors at embryonic day 7.0 to 8.0. With the use of this method, we found that knockdown of the chromatin-associated protein Hmga2 in NECs inhibited the onset of the neurogenic phase in the neocortex. This effect of Hmga2 knockdown was accompanied by inhibition of the expression of a set of genes targeted by Polycomb group proteins, which repress neurogenic genes in cortical progenitors. Our study thus establishes a novel method for manipulation of gene expression in the early stage of mouse brain development as well as uncovers a key molecular player in the generation of neurogenic progenitors in the developing mouse neocortex.

Introduction

The neocortex is the seat of higher cognitive function and has undergone evolutionary expansion in mammals. It originates from a pseudostratified sheet of neuroepithelium present at the anterior end of the neural plate before formation of the neural tube. In the course of neocortical development, neural progenitors undergo sequential waves of expansion, neurogenic and gliogenic phases (Gotz and Huttner, 2005; Hirabayashi and Gotoh, 2010; Kriegstein and Alvarez-Buylla, 2009; Mukhtar and Taylor, 2018). During the expansion phase, neural progenitors, also known as neuroepithelial cells (NECs), divide symmetrically to give rise to two progenitors per division (Rakic, 1995). This symmetric division increases the progenitor pool and results in lateral expansion of the neocortex. At the onset of neurogenesis in the mouse neocortex, NECs transform into neurogenic radial glial cells (RGCs), which mainly divide asymmetrically to give rise to one progenitor and one neuron or neuron-committed intermediate progenitor cell per division (Gao et al., 2014; Gotz and Huttner, 2005; Hartfuss et al., 2001; Miyata et al., 2002; Noctor et al., 2001). The elongated basal (radial) processes of RGCs also support the migration of newborn neurons to the pial surface, which results in radial expansion of the neocortex (Rakic, 1972). Clonal analysis of the mouse neocortex has revealed that a neurogenic RGC typically produces 8~9 cortical excitatory neurons through asymmetric division and then transforms into a gliogenic RGC (Gao et al., 2014). To avoid confusion, we will hereafter use the term neural stem-progenitor cells (NPCs) for both NECs and RGCs, given that many, if not all, of these cells are neural stem cells that self-renew and eventually produce both neurons and glial cells and that various nomenclatures are currently in use in the field.

The expansion-to-neurogenic phase (E-to-N) transition of NPC fate takes place at around embryonic day (E) 10 in the mouse neocortex. The timing of this E-to-N transition is key to determination of the number of neurons generated and the size of the cortex, given that the duration of the expansion phase determines the size of the founder NPC pool for corticogenesis. With regard to the mechanism of this transition, certain secreted (extrinsic) factors have been found to play a role, with one such factor being all-*trans* retinoic acid (atRA) released from the meninges. In mice, a reticulum of meningeal cells covers the neocortex between E9 and E10 (McLone and Bondareff, 1975) and secretes atRA, which promotes the onset of neurogenesis while suppressing

neuroepithelial elongation (Siegenthaler et al., 2009). Fibroblast growth factor (FGF) 10 is transiently expressed in anterior NPCs from E9.5 to E11.5 and, together with its receptor FGFR2, also promotes the E-to-N transition in the anterior portion of the neocortex (Sahara and O'Leary, 2009; K. Yoon et al., 2004). Moreover, an increase in oxygen concentration as a result of periventricular ingrowth of blood vessels from E10.5 to E12.5 also appears to be associated with the E-to-N transition (Lange et al., 2016). In addition to these extrinsic factors, cell-intrinsic programs likely regulate the E-to-N transition, given that in vitro cultures of mouse cortical NPCs as well as of human embryonic stem (ES) cell– or primate induced pluripotent stem (iPS) cell–derived NPCs undergo a directional transition from proliferative (symmetric) to differentiating (asymmetric) divisions (Eiraku et al., 2008; Gaspard et al., 2008; Otani et al., 2016; Qian et al., 1998; Shen et al., 2006; Shi et al., 2012). The molecular basis of cell-intrinsic programs that regulate the E-to-N transition of NPC fate (in particular, the timing of this transition) has remained largely unclear, however. Only a few candidate intracellular mechanisms, such as those involving Notch-Hes signaling and the BAF chromatin-remodeling complex (Anthony et al., 2005; Gaiano et al., 2000; Hatakeyama et al., 2004; Nguyen et al., 2018), have been proposed to date.

One possible reason that the molecular basis of the E-to-N transition has remained relatively unexplored compared with that of neurogenesis or gliogenesis later in development is the difficulty of gene manipulation at this early stage of brain development. At late embryonic stages (from ~E12), a gene of interest can be readily introduced into neocortical NPCs by in utero electroporation of plasmids (Tabata and Nakajima, 2001) or by injection of recombinant viruses into the ventricles. However, these methods cannot be applied to earlier stages before the E-to-N transition (such as at E8.0) because neural tube closure does not take place until E8.5 to E9.5 in the mouse forebrain (so there is no ventricle at E8.0) and the presumptive neocortex is too small to manipulate. Ultrasound-guided injection of viruses into the mouse nervous system at E8.5 was introduced to overcome this difficulty (Gaiano et al., 1999). However, this method requires an ultrasound backscatter microscopy system, and retrovirus injection with this approach at E8.5 frequently resulted in developmental defects of neural tube closure or death of the embryo (41 out of 54). We therefore set out to establish a new method that does not require costly equipment and which has a high survival rate without the induction of gross developmental defects.

A hallmark of NPCs in the neurogenic phase is their neurogenic potential—that is, they maintain an undifferentiated state but are able to differentiate into neurons in response to appropriate cues. The chromatin state of NPCs underlies this neurogenic potential (Kishi and Gotoh, 2018; Nakagawa et al., 2020; Tsuboi et al., 2019). Polycomb group (PcG) proteins temporarily suppress the expression of neurogenic genes in NPCs through histone modification during the neurogenic phase, and this suppression is relieved on neuronal differentiation (Albert et al., 2017; Fasano et al., 2007; Hirabayashi et al., 2009; Morimoto-Suzki et al., 2014; Pereira et al., 2010; Tsuboi et al., 2018). At later developmental stages (during the gliogenic phase), however, NPCs lose their neurogenic potential as a result of persistent (robust) repression of neurogenic genes mediated in part through polymerization of PcG proteins (Hirabayashi et al., 2009; Tsuboi et al., 2018). High mobility group A (Hmga) proteins 1 and 2 are also chromatin modifiers that contribute to neurogenic potential by regulating the expression of neurogenesis-related genes in NPCs during the neurogenic phase (Fujii et al., 2013; Kishi et al., 2012; Sakai et al., 2019). The levels of Hmga proteins in NPCs are high in the neurogenic phase but gradually decrease during later neocortical development (Kishi et al., 2012; Nishino et al., 2008; Sanosaka et al., 2008), with this decline accounting in part for the loss of neurogenic potential in gliogenic NPCs (Kishi et al., 2012). However, it has remained unknown whether Hmga proteins play a role in the E-to-N transition of NPC fate in the early embryonic mouse neocortex.

We here describe a new and simple method for the introduction of a gene of interest into ectodermal and endodermal cells of mouse embryos as early as E7.0 or E8.0. This method is based on in utero injection of viral vectors into amniotic fluid and is associated with a high survival rate without inducing gross developmental abnormalities. Moreover, as a proof of concept, we have identified a key regulator of the E-to-N transition with the use of this new method. We found that *Hmga2* expression in neocortical NPCs peaks at around the E-to-N transition (at E10), and that knockdown of Hmga2 from E8.0 delayed the onset of neurogenesis and shifted the transcriptional profile of NPCs at this transition closer to that in the expansion phase. Importantly, knockdown of Hmga2 from E8.0 attenuated the expression of a subset of PcG target genes in NPCs at E11.0. Our results suggest that an increase in Hmga2 expression triggers the onset of the neurogenic phase in part through activation of neurogenesis-related PcG target genes.

Results

Development of a simple and efficient method for manipulation of gene expression in mouse embryos before neural tube closure

To investigate the E-to-N transition in the mouse neocortex, we set out to develop a simple and efficient method for the introduction of a gene of interest before neural tube closure, ideally before E8.5. To this end, instead of the ultrasound microscopy system adopted in a previous study (Gaiano et al., 1999), we used an optical fiber to visualize the inner structure of the uterus including the amnion and embryo (Figure 1). Optical fiber–based visualization of the ventricles of embryos from E9.5 was previously described for targeted DNA injection and electroporation after neural tube closure (Matsui et al., 2011). We found that lighting with this system was sufficient to allow injection of a dye inside the amnion, although it was not possible to directly see the amnion within the uterus. We first injected carboxyfluorescein succinimidyl ester (CFSE), a cell-permeable dye that becomes fluorescent after reaction with intracellular proteins (Quah and Parish, 2010; Telley et al., 2016), into the uterus at E8.0 (Figure S1) To minimize possible damage caused by the injection, we inserted a sharpened capillary at the center of the uterus at an angle perpendicular to the uterine wall while it was positioned as shown in Figure 1d. We injected a small volume (~0.5 μl) of solution at a depth of 1 to 2 mm below the uterine wall, which reproducibly resulted in transfer of the solution into the amniotic fluid. The time of surgery is relatively short (~20 min) because of the simplicity of the method, which may contribute to the minimal damage caused to embryos. After 3 days (at E11.0), fluorescence microscopy without sectioning revealed that 77% of injected embryos were labeled with CFSE (Figure S1a and b). About 80% of embryos survived without gross developmental malformations at E11.0. We also injected CFSE into amniotic fluid at E7.0, which again yielded a high rate of embryo labeling (64%) and a high rate of survival without gross developmental malformation (89%) at E9.0 (Figure S1b).

We next performed gene introduction via retroviral vectors with this method. We first injected a concentrated suspension of a retrovirus encoding green fluorescent protein (GFP) into the uterus at E8.0, and we found that 89% of embryos survived without gross abnormalities and that 74% of embryos expressed GFP at E11.0 (Figure 2a and c). Injection of the retrovirus at E7.0 also yielded high rates of GFP-expressing

174 embryos and surviving embryos at E9.0 (Figure 2b and c). Flow cytometric analysis of
175 cortical tissue obtained from E12.0 embryos that had been injected with the retrovirus
176 for GFP at E8.0 showed that ~70% of the cortical cells were positive for GFP in
177 successful cases (Figure 2d). Immunohistofluorescence analysis of sagittal sections of
178 E10.0 embryos that had been injected with the retrovirus encoding GFP at E8.0 revealed
179 that most tissues exposed to amniotic fluid expressed GFP (Figure 2e–g). The labeled
180 tissues thus included the central nervous system (forebrain, midbrain, hindbrain, and
181 spinal cord) as well as the epidermis and endodermal tissues such as those of digestive
182 and respiratory organs. These results suggested that our method is also suitable for gene
183 introduction into such ectodermal and endodermal tissues at this early stage of mouse
184 development.
185 Given that in utero electroporation of plasmids is in general superior to
186 retroviral infection as a means of gene introduction with regard to efficiency and
187 expression level, we next injected a plasmid encoding mCherry with our new method
188 and performed in utero electroporation with the use of electrodes (disc size, 2.5 by 4
189 mm) positioned on each side of the uterus at E7.0 or E8.0. The fraction of mCherry-
190 expressing embryos at E9.0 and E10.0 was 19% and 40% among those electroporated at
191 E7.0 and E8.0, respectively (Figure S2a, b). The expression pattern of mCherry differed
192 among embryos, likely because of differences in the orientation of the electrodes
193 relative to the embryo during electroporation. Most embryos expressed mCherry in
194 somites (Figure S2a), whereas another manifested mCherry expression in the midbrain
195 and hindbrain (data not shown). No embryo examined to date was found to express
196 mCherry in the forebrain. These results showed that it was possible to perform gene
197 introduction by in utero electroporation in mouse embryos at E7.0 or E8.0 with our
198 method for plasmid injection, although further improvements will be necessary to allow
199 targeting of a specific tissue with this method.
200
201 **Transcriptional profiling of NPCs in the mouse telencephalon during early**
202 **development**
203 To investigate the molecular basis of the E-to-N transition, we first examined changes in
204 the transcriptional profile of NPCs around this developmental stage by RNA-
205 sequencing (RNA-seq) analysis. Given that the E-to-N transition takes place at ~E10 in
206 mice, we isolated NPCs as cells expressing the NPC marker CD133 (also known as

prominin-1) at a high level (CD133^{high} cells) from the entire telencephalon at E8.0 and E9.0 and from the neocortex at E10.0, E11.0, and E12.0 by fluorescence-activated cell sorting (FACS) (Figure 3a). Hierarchical clustering analysis of differentially expressed genes (defined by maSigPro of the R package) revealed five clusters based on the pattern of the expression changes (Figure 3b–f). The genes in cluster 1 showed a decline in expression level, most prominently from E8.0 to E10.0 (Figure 3b), whereas those in cluster 3 showed an increase in expression level, most prominently from E10.0 to E12.0 (Figure 3d). Gene ontology (GO) analysis showed that the genes in cluster 1 were enriched in those related to tissue morphogenesis and embryo development (Figure 3b), whereas the genes in cluster 3 were enriched in those related to nervous system development and generation of neurons (Figure 3d). These findings confirmed the proper isolation of NPCs at each stage. The genes in clusters 2 and 4 were potentially associated with the E-to-N transition (~E10), given that their expression levels decreased and increased, respectively, predominantly from E9.0 to E11.0 (Figure 3c and e). The genes in cluster 2 were enriched in those related to ribosome biogenesis and RNA processing (Figure 3c), suggesting that these processes might be regulated differentially in the expansion versus neurogenic phase. Ribosome biogenesis has indeed been found to be attenuated in NPCs at around this stage (Chau et al., 2018), again providing support for the proper isolation of NPCs for this analysis. The enrichment of genes related to RNA processing in cluster 2 is of interest, given the pivotal role of such processing in the control of NPC differentiation (K.-J. Yoon et al., 2017; Zahr et al., 2018; Zhang et al., 2016). The genes in cluster 4 were enriched in those related to cell projection and cell morphogenesis (Figure 3e), possibly reflecting the dynamic morphological changes of NPCs as they transition from NECs to RGCs.

The genes in cluster 5 may be particularly relevant to the E-to-N transition, given that their expression peaks at E10.0 (Figure 3f). We therefore hypothesized that this cluster includes genes that promote the E-to-N transition. The top five highly expressed genes of cluster 5 at E10.0 are shown in Figure 3g. Among them, we focused on *Hmga2*, given that Hmga proteins have been shown to confer neurogenic potential on mouse neocortical NPCs at late developmental stages (Kishi et al., 2012). However, the possible role of Hmga2 at early developmental stages—in particular, at the E-to-N transition—has remained unknown.

240 **Hmga2 promotes the onset of neurogenesis in the mouse neocortex**
241 We first confirmed the temporal expression pattern of *Hmga2* in NPCs by reverse
242 transcription and quantitative polymerase chain reaction (RT-qPCR) analysis, which
243 again showed a peak at E10.0 (Figure 3h). To investigate the relevance of this increase
244 in the level of *Hmga2* expression in neocortical NPCs at this particular embryonic stage,
245 we knocked down Hmga2 with the use of a specific short hairpin RNA (shRNA) from
246 E8.0 with our novel method for early embryo manipulation. We introduced retroviruses
247 encoding GFP and shRNAs specific either for Hmga2 or for luciferase (control) into
248 NPCs at E8.0 and analyzed the embryos at E10.0 and E11.0 (Figure 4a). RT-qPCR and
249 immunohistofluorescence analyses confirmed the depletion of *Hmga2* mRNA and
250 Hmga2 protein in NPCs at these stages for embryos infected with the retrovirus for
251 Hmga2 shRNA at E8.0 (Figure 4b and c). We then examined the effect of Hmga2
252 knockdown on neurogenesis by immunostaining for Tbr2, a marker of intermediate
253 neuronal progenitors and immature neurons (Englund et al., 2005). Whereas Hmga2
254 knockdown from E8.0 did not affect the fraction of Tbr2-positive cells among GFP-
255 positive cells at E10.0, it significantly attenuated the increase in the fraction of such
256 cells apparent at E11.0 (Figure 4d and e). In contrast, Hmga2 knockdown from E8.0 did
257 not significantly affect the fraction of cells positive for Sox2, an NPC marker (Ellis et
258 al., 2004), among GFP-positive cells at E11.0 (Figure 4f and g). These results suggested
259 that Hmga2 promotes neurogenesis in neocortical NPCs at the onset of the neurogenic
260 phase.
261 There were at least two possible explanations for the attenuation of
262 neurogenesis by knockdown of Hmga2: Hmga2 might promote the E-to-N transition of
263 NPCs, in which case Hmga2 depletion would be expected to prolong the expansion
264 phase and delay the start of the neurogenic phase; or Hmga2 might promote neuronal
265 differentiation of NPCs during the neurogenic phase without affecting the E-to-N
266 transition of NPCs. To discriminate between these possibilities, we examined whether
267 Hmga2 knockdown might delay the developmental change in the transcriptional profile
268 of neocortical NPCs at the E-to-N transition. We therefore introduced retroviruses
269 encoding GFP and either control or Hmga2 shRNAs into embryos at E8.0 and isolated
270 GFP-expressing CD133^{high} neocortical NPCs by FACS at E10.0 or E11.0 for RNA-seq
271 analysis, which we performed with the Quartz-seq method for analysis of a small
272 number of cells (Sasagawa et al., 2013) (Figure 5a). The expression of *Hmga2* as well

273 as that of *Igf2bp2*, a target gene of Hmga2 in NPCs (Fujii et al., 2013), were found to be
274 greatly reduced in NPCs of embryos infected with the retrovirus for Hmga2 shRNA
275 (Figure 5b), thus confirming the efficient knockdown of Hmga2 by this procedure. We
276 then performed gene set enrichment analysis (GSEA) to compare the expression levels
277 of signature genes of NPCs in the expansion phase between control and Hmga2-
278 depleted NPCs at E10.0. We examined genes in cluster 2 as such signature genes, given
279 the prominent decline in their expression level from E9.0 to E11.0 (Figure 3c), and we
280 found that their expression level was significantly higher (enriched) in Hmga2-depleted
281 NPCs than in control NPCs (Figure 5c). This finding suggested that Hmga2 knockdown
282 shifts the transcriptional profile of NPCs closer to that apparent in the expansion phase,
283 providing support for the notion that the observed increase in Hmga2 expression
284 promotes the E-to-N transition of NPC fate in the neocortex. We previously showed that
285 Hmga2 knockdown during the late neurogenic phase did not promote premature
286 neuronal differentiation (Kishi et al., 2012), which further supports the notion that
287 Hmga2 promotes the E-to-N transition of NPC fate rather than neuronal differentiation
288 of NPCs per se.
289 Of interest, Hmga2 knockdown from E8.0 did not significantly increase the
290 fraction of NPCs positive for phosphorylated histone H3 at E11.0 (data not shown),
291 suggesting that Hmga2 might not overtly contribute to the change in cell division rate
292 associated with the E-to-N transition. Together, our results thus implicated Hmga2 in
293 changes in some (including the acquisition of neurogenic potential) but not all
294 properties of NPCs related to this transition.
295
296 **Hmga2 activates a subset of PcG target genes in early-stage neocortical NPCs**
297 How does Hmga2 promote the acquisition of neurogenic potential in NPCs (without
298 promoting neuronal differentiation per se)? In the developing mouse neocortex as well
299 as in other contexts, PcG proteins have been shown to determine neurogenic potential
300 through transient repression of neurogenic genes (Fasano et al., 2007; Hirabayashi et al.,
301 2009; Mikkelsen et al., 2007; Mohn et al., 2008; Morimoto-Suzki et al., 2014; Pereira et
302 al., 2010; Tsuboi et al., 2018). We then asked whether there is any relation between
303 Hmga2 and PcG proteins in NPCs at the early stage of neocortical development. Given
304 that PcG proteins catalyze histone modification including trimethylation at lysine-27 of
305 histone H3 (H3K27me3), we performed chromatin immunoprecipitation (ChIP)-seq

analysis of Hmga2 and H3K27me3 in neocortical cells at E11.0. Clustering analysis (and a heat map with Jaccard index) showed that loci associated with H3K27me3 showed an inverse correlation with those associated with Hmga2 in these cells (Figure 6a), consistent with a previous finding in mouse ES cells (Colombo et al., 2017). This exclusive binding pattern may be due in large part to the preferential binding of Hmga2 and PcG proteins to AT-rich and GC-rich sequences, respectively (Colombo et al., 2017; Ku et al., 2008; H. Li et al., 2017; Winter et al., 2011), but it was also possible that these molecules interact functionally. We therefore examined whether knockdown of Hmga2 in NPCs might affect the expression of PcG target genes, which we defined in this study as genes that were derepressed (up-regulated) in response to ablation of Ring1B, an essential component of PcG protein complexes. We first examined a set of PcG target genes that we previously identified in a primary culture of NPCs prepared from E18 mouse neocortex (Hirabayashi et al., 2009). GSEA of our Quartz-seq data (Figure 5) showed that these PcG target genes were expressed at a significantly higher level in control NPCs than in Hmga2-depleted NPCs at E11.0 (Figure 6b). We next examined another set of PcG target genes that we identified in neocortical NPCs in vivo by conditional deletion of *Ring1b* from E15 to E18 against a background of *Ring1a* deletion (with the use of *Ring1a*$^{-/-}$;*Ring1b*$^{flox/flox}$;*Rosa-CreERT2*$^{-/-\ or\ +/-}$ mouse embryos). Again, GSEA revealed that these PcG target genes were expressed at a significantly higher level in control NPCs than in Hmga2-knockdown NPCs at E11.0 (Figure 6c). These results thus suggested that Hmga2 promotes the expression of (at least some) PcG target genes in NPCs, with this effect possibly underlying the function of Hmga2 in conferring neurogenic potential on these cells. Finally, we performed GO analysis of core enriched genes whose expression was derepressed by Ring1B ablation and down-regulated by Hmga2 knockdown (Figure 6b and 6c). The top hits of this analysis included brain development and nervous system development (Figure 6d), providing further support for the notion that Hmga2 promotes the expression of PcG target genes that contribute to nervous system development.

Discussion

A directional transition of NPC fate from the expansion phase to the neurogenic phase takes place during mammalian brain development, but the cell-intrinsic programs that govern this transition have remained largely unclear. We have here investigated changes in the transcriptional profile of mouse neocortical NPCs, and we identified gene sets that are specifically up- or down-regulated around the time of this E-to-N transition. Among the highly expressed genes whose expression peaks around this transition, we focused on that for the chromatin-associated protein Hmga2 and examined the effects of its knockdown with the use of a new method we developed in this study for the genetic manipulation of early-stage NPCs before neural tube closure. We thus found that forced depletion of Hmga2 in neocortical NPCs from E8.0 hindered the increase in neurogenesis apparent at the onset of the neurogenic phase (from E10.0 to E11.0). Moreover, we found that this effect of Hmga2 depletion was likely due to a delay in the E-to-N transition of NPC fate rather than to inhibition of neuronal differentiation per se within the neurogenic phase, given the delayed change in the transcriptional profile of NPCs induced by the loss of Hmga2. Importantly, the genes whose expression was attenuated in Hmga2-depleted NPCs were enriched in PcG target genes (genes up-regulated by deletion of *Ring1b*) in these cells. On the basis of our results, we propose that the increase in Hmga2 expression apparent at the E-to-N transition facilitates the expression of a subset of PcG target genes and thereby promotes this transition of NPC fate—in particular, by promoting the acquisition of neurogenic potential.

Investigation of the molecular mechanism underlying the E-to-N transition of NPC fate in any detail requires manipulation of gene expression before neural tube closure. However, existing (convenient and simple) methods such as injection into the ventricles of viruses or of plasmids for in utero electroporation (Tabata and Nakajima, 2001) can be applied only after neural tube closure. The method for gene introduction developed in the present study has several advantages over other methods that can be used before neural tube closure, such as whole-embryo genomic manipulation (gene targeting or transgene introduction) and ultrasound-guided injection of viruses into the mouse nervous system. Whereas genomic manipulation requires a specific Cre-expressing mouse line or knowledge of specific distal elements to control expression of a gene of interest in a temporally and spatially regulated manner, our new method

369 allows expression of a gene of interest in NPCs as well as in other ectodermal or
370 endodermal cells before neural tube closure without such mouse lines or knowledge.
371 Our method is also less costly, less labor-intensive, and less time-consuming compared
372 with existing methods and is thus suitable for testing and screening a large number of
373 genes for their specific effects. The relatively simple and rapid nature of our procedure
374 also appears to be beneficial in terms of minimizing developmental abnormalities and
375 maximizing the survival rate of manipulated embryos compared with the ultrasound-
376 guided injection of viruses (Gaiano et al., 1999). Given that many recent studies based
377 on brain organoids have implicated various molecules as potential regulators of early
378 brain development, a simple and efficient method for gene introduction into early-stage
379 mouse NPCs would be useful for rapid testing of the functions of these molecules in the
380 in vivo context.

381 Our present results suggest that Hmga2 positively regulates the expression of
382 PcG target genes in neocortical NPCs. PcG proteins are known to repress a specific
383 subset of developmental genes in a context-dependent manner, but the mechanisms
384 underlying this context-dependent regulation remain obscure in many cases. Our
385 findings now implicate Hmga2 as a factor that, directly or indirectly, regulates PcG
386 protein function in a locus- and developmental stage–dependent manner. It remains
387 unclear, however, how Hmga2 may regulate PcG target genes. Regulation of certain
388 genes (such as *CcnA2*, *Igf2bp2*, and *Plag1*) through direct association of Hmga2 with
389 their promoters has been described (Cleynen et al., 2007; Z. Li et al., 2012; Sakai et al.,
390 2019; Tessari et al., 2003; Vignali and Marracci, 2020), but this mechanism of
391 regulation seems to be relatively minor given the global exclusion of Hmga2 from gene
392 promoters in mouse ES cells (Colombo et al., 2017). Although Hmga2 has been
393 proposed to compete with histone H1 for linker DNA and thereby to open chromatin
394 (Catez et al., 2004), direct evidence for such a mechanism is lacking. Further
395 biochemical and cellular studies will be necessary to characterize the precise role of
396 Hmga2 in the regulation of its target genes.

397 Given the proposed function of Hmga2 as a trigger of the E-to-N transition,
398 the timing of the increase in Hmga2 abundance may play an important role in
399 determining that of the E-to-N transition. We indeed found that the amount of *Hmga2*
400 mRNA peaks at around the time of this transition (at ~E10) in mouse neocortical NPCs.
401 Then, what upstream pathways (mechanisms) might regulate this increase of *Hmga2*

402 expression? It is possible that extrinsic factors implicated in the E-to-N transition in the
403 mouse neocortex, such as FGF10 and atRA, contribute to the regulation of *Hmga2*
404 expression. Of note, the promoter of the mouse *Hmga2* gene contains putative retinoic
405 acid–responsive elements that are able to bind retinoic acid receptors (data not shown).
406 Myc proteins as well as the Lin28–*let7* microRNA axis have also been shown to
407 promote the expression of *Hmga2* in other cell types (Chang et al., 2009; Copley et al.,
408 2013; Lee and Dutta, 2007; Mayr et al., 2007). Although we did not detect an increase
409 in the expression of Myc-family proteins around E9 to E11, we found that the level of
410 *Lin28b* mRNA increases in neocortical NPCs before that of *Hmga2* mRNA at around
411 this time of development (data not shown). It will therefore be of interest to examine the
412 relevance of Lin28 to the regulation of *Hmga2* expression in the context of the E-to-N
413 transition in the mouse neocortex.
414 The search for the "timer" of the E-to-N transition is especially relevant to our
415 understanding of the evolutionary enlargement of the brain, given that the duration of
416 the expansion phase (or the number of symmetric NPC divisions) is expected to
417 positively correlate with the size of the founder NPC pool. Indeed, the enlargement of
418 the neocortex in primates as compared with rodents appears to be related to lengthening
419 of the expansion phase from a few days to several weeks (Dehay et al., 2015; Kornack
420 and Rakic, 1998; Rakic, 2009; 1995) in addition to the emergence of additional
421 proliferative NPC populations (such as outer/basal RGCs) (Betizeau et al., 2013; Fietz
422 et al., 2010; Hansen et al., 2010) and the continuation of proliferative NPC divisions
423 even after the onset of neurogenesis (Otani et al., 2016). Even among primates, the cell-
424 autonomous timing of the E-to-N transition in cultured NPCs is delayed in humans
425 compared with nonhuman primates (Otani et al., 2016). Of interest, the level of *HMGA2*
426 mRNA also seems to be high in neocortical NPCs at around the onset of neurogenesis
427 (gestation week 7 to 8) during early human development (Nowakowski et al., 2017).
428 Moreover, *HMGA2* was found to be one of the genes that most markedly influence the
429 velocity stream associated with timing of NPC fate transition at the early stage of
430 human neocortical development (Eze et al., 2020), suggesting the possibility that
431 HMGA2 plays a conserved role in the onset of the neurogenic phase in humans. If this
432 is the case, the difference in the regulation of Hmga2 gene expression between mouse
433 and human may provide insight into the timing of this transition.

The size of the neocortex is strictly regulated during mammalian development, with disorders that result from defects in such regulation in humans, such as macrocephaly and microcephaly, being associated with pathological or psychiatric conditions such as epilepsy, autism spectrum disorder, and schizophrenia (Sun and Hevner, 2014). A single-cell transcriptomic analysis of human neocortical progenitors indicated that genes that drive the early-stage transition of NPC fate are enriched in those associated with neurodevelopmental or psychiatric disorders (Eze et al., 2020). It will thus be of interest to investigate the impact of Hmga2 and its related molecules on neocortical size and, ultimately, neocortical function.

445 **Materials and Methods**

446

447 **Mouse maintenance**

448 All animals were studied according to protocols approved by the Animal Care and Use
449 Committee of The University of Tokyo. *Ring1a*$^{-/-}$;*Ring1b*$^{flox/flox}$ mice (Calés et al., 2008;
450 Endoh et al., 2008) were crossed with *Rosa26-CreERT2* mice (Taconic), in which
451 expression of *CreERT2* is driven by the endogenous *Rosa26* promoter. All mice were
452 maintained in a temperature- and relative humidity–controlled (23° ± 3°C and 50 ±
453 15%, respectively) environment with a normal 12-h-light, 12-h-dark cycle. Two to six
454 mice were housed per sterile cage (Innocage, Innovive; or Micro BARRIER Systems,
455 Edstrom Japan) containing bedding chips (PALSOFT, Oriental Yeast; or PaperClean,
456 SLC Japan), and they were provided with irradiated food (CE-2, CLEA Japan) and
457 filtered water ad libitum. For in utero injection before neural tube closure, mice were
458 allowed to mate for 2 h and the female was then checked for a vaginal plug. The time of
459 plug confirmation was defined as E0.0. For induction of CreERT2 activity, pregnant
460 mice were injected intraperitoneally with 150 μl of tamoxifen (Sigma) dissolved in
461 sunflower oil (Nacalai) at a concentration of 10 mg/ml.

462

463 **In utero injection and electroporation before neural tube closure**

464 Jcl:ICR (CLEA Japan) or Slc:ICR (SLC Japan) mice were used for in utero injection
465 experiments. Pregnant mice were injected intraperitoneally with a sodium
466 pentobarbital–based anesthetic, and the uterine horn was exposed and pinched between
467 a flexible fiber-optic cable and a finger (Matsui et al., 2011). Lighting from the fiber-
468 optic cable allowed visualization of the internal uterine structure but did not allow the
469 embryo to be distinguished from the amnion. A small volume (~0.5 μl) of CFSE (1 mM,
470 Sigma), plasmid DNA (1 μg/μl), or retroviruses, each mixed with FastGreen (Chroma
471 Gesellschaft), was injected with a sharpened capillary at an angle perpendicular to the
472 center of the uterus. An injection depth of 1 to 2 mm below the uterine wall allowed the
473 reproducible introduction of the capillary contents into amniotic fluid. For
474 electroporation, the uterus was held between the tweezer-type electrodes
475 (CUY652P2.5x4, Nepa Gene) and electroporated with a NEPA21 system (Nepa Gene)
476 according to the following program: three poring pulses of 30 V with a 15-ms pulse
477 width and 450-ms pulse interval and 10% decay (+ pulse orientation), and two transfer

478 pulses of 10 V with a 50-ms pulse width and 450-ms pulse interval and 10% decay (±
479 pulse orientation). After the injection and electroporation were completed, the uterine
480 horn was placed back into its original location. Embryos were imaged with a
481 fluorescence stereo microscope (2.0× lens, Nikon SMZ18).
482
483 **Plasmid construction**
484 The cDNA for mCherry was cloned by PCR, and its coding sequence was verified by
485 DNA sequencing. The cDNA was subcloned into pCAGEN (a kind gift from C. L.
486 Cepko) to generate the pCAGEN-mCherry plasmid.
487
488 **Retrovirus production and concentration**
489 Retroviruses were produced by transfection of PLAT-GP cells (a kind gift from T.
490 Kitamura) with the previously validated retroviral vectors pSIREN-siLuc (for control
491 shRNA, Addgene #122287) or pSIREN-siHmga2 (for Hmga2 shRNA, Addgene
492 #122290) (Kishi et al., 2012) and with a VSVG plasmid (a kind gift from H. Song).
493 Conditioned medium collected 72 h after the onset of transfection was cleared of debris
494 by centrifugation at 2500 × *g* for 5 min, passed through a 0.45-μm filter, and centrifuged
495 at 250,000 × *g* for 90 min at 4°C and then at 20,000 × *g* for >12 h at 4°C. The resulting
496 virus pellet was suspended in phosphate-buffered saline (PBS). For in utero injection,
497 10 ml of conditioned medium from PLAT-GP cells in a 10-cm dish was concentrated
498 into 10 μl of PBS.
499
500 **Flow cytometry and FACS**
501 The telencephalon or neocortex of ICR embryos was dissected and subjected to
502 enzymatic digestion with a papain-based solution (Sumitomo Bakelite). For
503 quantification of the efficiency of gene introduction, the cells were directly subjected to
504 flow cytometric analysis with a FACS Aria instrument (Becton Dickinson). For
505 isolation of NPCs, the cells were stained with allophycocyanin-conjugated antibodies to
506 CD133 (1:400 dilution, BioLegend 141210) and sorted with a FACS Aria instrument
507 (Becton Dickinson). The threshold of CD133 intensity for selection of NPCs was set as
508 follows: E8.0, top 80%; E9.0, top 70%; E10.0, top 60%; E11.0, top 50%; and E12.0, top
509 50%.
510

511 **Immunohistofluorescence analysis**

512 Immunohistofluorescence staining was performed as previously described (Morimoto-
513 Suzki et al., 2014), with minor modifications including fixation for 3 h without
514 perfusion and the use of a blocking buffer comprising 0.1% Triton X-100 and 3%
515 bovine serum albumin. Primary antibodies and dilutions for immunostaining were as
516 follows: anti-Hmga2, 1:500 (Cell Signaling); anti-Sox2, 1:500 (Cell Signaling); anti-
517 Tbr2, 1:500 (chick, Millipore); anti–phospho-histone H3, 1:500 (Cell Signaling); and
518 anti-GFP, 1:2000 (Abcam) or 1:1000 (Nakalai). Images were acquired with a laser-
519 scanning confocal microscope (TSC-SP5, Leica) and ImageJ software (NIH). For
520 quantification, the average value of multiple sections of the telencephalon along the
521 rostrocaudal axis was determined for each embryo.

522

523 **RT-qPCR analysis**

524 Total RNA was isolated from cells with the use of RNAiso plus (Takara), and up to 0.5
525 μg of the RNA was subjected to RT with the use of ReverTra Ace qPCR RT Master Mix
526 with gDNA remover (Toyobo). The resulting cDNA was subjected to real-time PCR
527 analysis in a LightCycler 480 instrument (Roche) with either KAPA SYBR FAST for
528 LightCycler 480 (Kapa Biosystems) or Thunderbird SYBR qPCR Mix (Toyobo). The
529 amount of each target mRNA was normalized by that of *Actb* mRNA. Primer sequences
530 were described previously (Sakai et al., 2019).

531

532 **RNA-seq analysis**

533 Libraries for RNA-seq analysis were constructed from total RNA isolated as for RT-
534 qPCR analysis. An Illumina TruSeq RNA sample preparation kit was used for template
535 preparation, which was followed by deep sequencing on the Illumina HiSeq platform to
536 obtain 36-base single-end reads. Approximately 20 million sequences were obtained.
537 Sequenced reads of NPCs isolated from wild-type embryos or from Ring1A/B knockout
538 embryos were mapped to the reference mouse genome mm10 or mm9 with the use of
539 Hisat2 (Kim et al., 2019) or ELAND (Illumina), respectively. Only uniquely mapped
540 and "deduplicated" reads with no base mismatch were used. Expression information
541 was obtained as RPKM based on the RefSeq gene models and with the use of
542 featureCounts (Liao et al., 2014). Gene clustering analysis based on expression patterns

543 was performed with maSigPro (Conesa et al., 2006). GO analysis for functional
544 annotation was conducted with DAVID software (Huang et al., 2009).
545
546 **Quartz-seq analysis**
547 Both cDNA synthesis and amplification were performed with total RNA from 1000
548 cells as described previously (Sasagawa et al., 2013). The amplified cDNA was
549 prepared for sequencing with the use of a Nextera XT DNA Sample Prep Kit (Illumina)
550 and was subjected to deep sequencing analysis on the Illumina HiSeq platform to yield
551 36-base single-end reads. Approximately 2 million sequences were obtained from each
552 sample. Sequences were mapped to the reference mouse genome (mm10) with Hisat2
553 (Kim et al., 2019). Only uniquely mapped and "deduplicated" reads with no base
554 mismatch were used. Gene expression was quantitated as RPKM on the basis of RefSeq
555 gene models (mm10) with the use of featureCounts (Liao et al., 2014).
556
557 **GSEA**
558 Enrichment of signature genes was assessed with GSEA software (Subramanian et al.,
559 2005). Each gene set was determined as follows. Expansion-phase genes: genes
560 expressed in cluster 2 at ≥50 RPKM at E9.0. Ring1B target genes in cultured NPCs:
561 Ring1B knockout (KO)/control ≥ 1.5, expression in control ≥ 3.0 RPKM (Hirabayashi
562 et al., 2009). Ring1B target genes in NPCs in vivo: Ring1A/B KO/Ring1A KO ≥ 3.0,
563 expression in control (Ring1A KO) ≥ 1.0 RPKM.
564
565 **ChIP-seq analysis**
566 ChIP analysis was performed as previously described (Sakai et al., 2019) with
567 antibodies to Hmga2 (Cell Signaling) and to H3K27me3 (MBL). Two million cells
568 directly isolated from the neocortex of embryos at E11.0 were used for ChIP-seq of
569 Hmga2, and 100,000 NPCs isolated as CD133^{high} cells by FACS from the neocortex of
570 embryos at E11.0 were used for ChIP-seq of H3K27me3. An Illumina TruSeq DNA
571 sample preparation kit was used for template preparation, which was followed by deep
572 sequencing analysis on the Illumina HiSeq platform to obtain 36-base single-end reads.
573 Sequences were mapped to the reference mouse genome (mm10) with bowtie software
574 (Langmead et al., 2009). Only uniquely mapped reads without blacklist regions
575 determined by the ENCODE project (Amemiya et al., 2019) were used. Peaks for

576 Hmga2 and H3K27me3 were called with the use of F-seq software (Boyle et al., 2008).
577 Jaccard indices for sample comparisons were determined with bedtools (Quinlan and
578 Hall, 2010). R was used for clustering and heat map construction.
579
580 **Statistical analysis**
581 Data presented as means + SEM were compared with the two-tailed Student's paired or
582 Welch's *t* test or by one-way analysis of variance (ANOVA) followed by the
583 Bonferroni-Holm multiple-comparison test. A p value of <0.05 was considered
584 statistically significant.
585
586

587 **Acknowledgments**
588 We thank T. Shimogori (RIKEN) as well as M. Miura, Y. Yamaguchi, K. Hashimoto,
589 and H. Miyazawa (The University of Tokyo) for technical advice regarding in utero
590 injection before neural tube closure; I. Nikaido (RIKEN) for advice on Quartz-seq
591 analysis; K. Imamura, T. Horiuchi, and S. Sugano (The University of Tokyo) for
592 assistance with high-throughput sequencing analysis; Y. Koseki (RIKEN) for providing
593 *Ring1* mutant mice; H. Song (Johns Hopkins University School of Medicine, Baltimore,
594 MD) for the plasmid encoding the VSVG; T. Kitamura (The University of Tokyo) for
595 PLAT-GP cells; C. L. Cepko (Harvard Medical School) for the pCAGEN plasmid; The
596 One-Stop Sharing Facility Center for Future Drug Discoveries (The University of
597 Tokyo) for FACS; R. Nagayoshi, and Y. Kakeya (The University of Tokyo) for
598 technical assistance; and members of the Gotoh laboratory for discussion. This research
599 was supported by AMED-CREST (JP20gm1310004 to Y.G.), by AMED-PRIME
600 (JP20gm6110021 to Y.K.), and by MEXT/JSPS KAKENHI (JP16H06481 and
601 JP16H06479 to Y.G.; JP19H05253, JP20H03179, JP20H05383, and JP16H06279 to
602 Y.K.).
603
604 **Author Contributions**
605 N.K., Y.K., Y.H. and Y.G. designed the study and wrote the manuscript. N.K., Y.K.,
606 Y.M., Y.N., and Y.H. performed the experiments and analyzed the data. Y.S. performed
607 high-throughput sequencing analysis. H.K. generated *Ring1a*$^{-/-}$;*Ring1b*$^{flox/flox}$ mice.
608 Y.K., Y.H., and Y.G. supervised the study.
609
610 **Declaration of Interests**
611 The authors declare no competing interests.
612

613 **References**

614

615 Albert, M., Kalebic, N., Florio, M., Lakshmanaperumal, N., Haffner, C., Brandl, H.,
616 Henry, I., Huttner, W.B., 2017. Epigenome profiling and editing of neocortical
617 progenitor cells during development. The EMBO Journal 36, 2642–2658.
618 doi:10.15252/embj.201796764
619 Amemiya, H.M., Kundaje, A., Boyle, A.P., 2019. The ENCODE Blacklist:
620 Identification of Problematic Regions of the Genome. Sci Rep 9, 9354–5.
621 doi:10.1038/s41598-019-45839-z
622 Anthony, T.E., Mason, H.A., Gridley, T., Fishell, G., Heintz, N., 2005. Brain lipid-
623 binding protein is a direct target of Notch signaling in radial glial cells. Genes &
624 Development 19, 1028–1033. doi:10.1101/gad.1302105
625 Betizeau, M., Cortay, V., Patti, D., Pfister, S., Gautier, E., Bellemin-Ménard, A.,
626 Afanassieff, M., Huissoud, C., Douglas, R.J., Kennedy, H., Dehay, C., 2013.
627 Precursor diversity and complexity of lineage relationships in the outer
628 subventricular zone of the primate. Neuron 80, 442–457.
629 doi:10.1016/j.neuron.2013.09.032
630 Boyle, A.P., Guinney, J., Crawford, G.E., Furey, T.S., 2008. F-Seq: a feature density
631 estimator for high-throughput sequence tags. Bioinformatics 24, 2537–2538.
632 doi:10.1093/bioinformatics/btn480
633 Calés, C., Roman-Trufero, M., Pavón, L., Serrano, I., Melgar, T., Endoh, M., Pérez, C.,
634 Koseki, H., Vidal, M., 2008. Inactivation of the polycomb group protein Ring1B
635 unveils an antiproliferative role in hematopoietic cell expansion and cooperation
636 with tumorigenesis associated with Ink4a deletion. Molecular and Cellular Biology
637 28, 1018–1028. doi:10.1128/MCB.01136-07
638 Catez, F., Yang, H., Tracey, K.J., Reeves, R., Misteli, T., Bustin, M., 2004. Network of
639 dynamic interactions between histone H1 and high-mobility-group proteins in
640 chromatin. Molecular and Cellular Biology 24, 4321–4328.
641 doi:10.1128/mcb.24.10.4321-4328.2004
642 Chang, T.-C., Zeitels, L.R., Hwang, H.-W., Chivukula, R.R., Wentzel, E.A., Dews, M.,
643 Jung, J., Gao, P., Dang, C.V., Beer, M.A., Thomas-Tikhonenko, A., Mendell, J.T.,
644 2009. Lin-28B transactivation is necessary for Myc-mediated let-7 repression and
645 proliferation. Proceedings of the National Academy of Sciences 106, 3384–3389.

646 doi:10.1073/pnas.0808300106
647 Chau, K.F., Shannon, M.L., Fame, R.M., Fonseca, E., Mullan, H., Johnson, M.B.,
648 Sendamarai, A.K., Springel, M.W., Laurent, B., Lehtinen, M.K., 2018.
649 Downregulation of ribosome biogenesis during early forebrain development. Elife
650 7. doi:10.7554/eLife.36998
651 Cleynen, I., Brants, J.R., Peeters, K., Deckers, R., Debiec-Rychter, M., Sciot, R., Van
652 De Ven, W.J.M., Petit, M.M.R., 2007. HMGA2 regulates transcription of the Imp2
653 gene via an intronic regulatory element in cooperation with nuclear factor-kappaB.
654 Mol. Cancer Res. 5, 363–372. doi:10.1158/1541-7786.MCR-06-0331
655 Colombo, D.F., Burger, L., Baubec, T., Schübeler, D., 2017. Binding of high mobility
656 group A proteins to the mammalian genome occurs as a function of AT-content.
657 PLoS Genet 13, e1007102–36. doi:10.1371/journal.pgen.1007102
658 Conesa, A., Nueda, M.J., Ferrer, A., Talón, M., 2006. maSigPro: a method to identify
659 significantly differential expression profiles in time-course microarray experiments.
660 Bioinformatics 22, 1096–1102. doi:10.1093/bioinformatics/btl056
661 Copley, M.R., Babovic, S., Benz, C., Knapp, D.J.H.F., Beer, P.A., Kent, D.G., Wohrer,
662 S., Treloar, D.Q., Day, C., Rowe, K., Mader, H., Kuchenbauer, F., Humphries,
663 R.K., Eaves, C.J., 2013. The Lin28b-let-7-Hmga2 axis determines the higher self-
664 renewal potential of fetal haematopoietic stem cells. Nature Cell Biology.
665 doi:10.1038/ncb2783
666 Dehay, C., Kennedy, H., Kosik, K.S., 2015. The outer subventricular zone and primate-
667 specific cortical complexification. Neuron 85, 683–694.
668 doi:10.1016/j.neuron.2014.12.060
669 Eiraku, M., Watanabe, K., Matsuo-Takasaki, M., Kawada, M., Yonemura, S.,
670 Matsumura, M., Wataya, T., Nishiyama, A., Muguruma, K., Sasai, Y., 2008. Self-
671 organized formation of polarized cortical tissues from ESCs and its active
672 manipulation by extrinsic signals. Cell Stem Cell 3, 519–532.
673 doi:10.1016/j.stem.2008.09.002
674 Ellis, P., Fagan, B.M., Magness, S.T., Hutton, S., Taranova, O., Hayashi, S., McMahon,
675 A., Rao, M., Pevny, L., 2004. SOX2, a persistent marker for multipotential neural
676 stem cells derived from embryonic stem cells, the embryo or the adult. Dev.
677 Neurosci. 26, 148–165. doi:10.1159/000082134
678 Endoh, M., Endo, T.A., Endoh, T., Fujimura, Y.-I., Ohara, O., Toyoda, T., Otte, A.P.,

679 Okano, M., Brockdorff, N., Vidal, M., Koseki, H., 2008. Polycomb group proteins
680 Ring1A/B are functionally linked to the core transcriptional regulatory circuitry to
681 maintain ES cell identity. Development 135, 1513–1524. doi:10.1242/dev.014340
682 Englund, C., Fink, A., Lau, C., Pham, D., Daza, R.A.M., Bulfone, A., Kowalczyk, T.,
683 Hevner, R.F., 2005. Pax6, Tbr2, and Tbr1 are expressed sequentially by radial glia,
684 intermediate progenitor cells, and postmitotic neurons in developing neocortex.
685 Journal of Neuroscience 25, 247–251. doi:10.1523/JNEUROSCI.2899-04.2005
686 Eze, U.C., Bhaduri, A., Nowakowski, T.J., Kriegstein, A., 2020, n.d. Heterogeneity of
687 Human Neuroepithelial Cells and Early Radial Glia. biorxiv.
688 doi:10.1101/2020.03.06.981423
689 Fasano, C.A., Dimos, J.T., Ivanova, N.B., Lowry, N., Lemischka, I.R., Temple, S.,
690 2007. shRNA knockdown of Bmi-1 reveals a critical role for p21-Rb pathway in
691 NSC self-renewal during development. Cell Stem Cell 1, 87–99.
692 doi:10.1016/j.stem.2007.04.001
693 Fietz, S.A., Kelava, I., Vogt, J., Wilsch-Bräuninger, M., Stenzel, D., Fish, J.L., Corbeil,
694 D., Riehn, A., Distler, W., Nitsch, R., Huttner, W.B., 2010. OSVZ progenitors of
695 human and ferret neocortex are epithelial-like and expand by integrin signaling.
696 Nature Neuroscience 13, 690–699. doi:10.1038/nn.2553
697 Fujii, Y., Kishi, Y., Gotoh, Y., 2013. IMP2 regulates differentiation potentials of mouse
698 neocortical neural precursor cells. Genes to Cells 18, 79–89. doi:10.1111/gtc.12024
699 Gaiano, N., Kohtz, J.D., Turnbull, D.H., Fishell, G., 1999. A method for rapid gain-of-
700 function studies in the mouse embryonic nervous system. Nature Neuroscience 2,
701 812–819. doi:10.1038/12186
702 Gaiano, N., Nye, J.S., Fishell, G., 2000. Radial glial identity is promoted by Notch1
703 signaling in the murine forebrain. Neuron 26, 395–404. doi:10.1016/s0896-
704 6273(00)81172-1
705 Gao, P., Postiglione, M.P., Krieger, T.G., Hernandez, L., Wang, C., Han, Z., Streicher,
706 C., Papusheva, E., Insolera, R., Chugh, K., Kodish, O., Huang, K., Simons, B.D.,
707 Luo, L., Hippenmeyer, S., Shi, S.-H., 2014. Deterministic progenitor behavior and
708 unitary production of neurons in the neocortex. Cell 159, 775–788.
709 doi:10.1016/j.cell.2014.10.027
710 Gaspard, N., Bouschet, T., Hourez, R., Dimidschstein, J., Naeije, G., van den Ameele,
711 J., Espuny-Camacho, I., Herpoel, A., Passante, L., Schiffmann, S.N., Gaillard, A.,

712 Vanderhaeghen, P., 2008. An intrinsic mechanism of corticogenesis from
713 embryonic stem cells. Nature 455, 351–357. doi:10.1038/nature07287
714 GOtz, M., Huttner, W.B., 2005. The cell biology of neurogenesis. Nat Rev Mol Cell
715 Biol 6, 777–788. doi:10.1038/nrm1739
716 Hansen, D.V., Lui, J.H., Parker, P.R.L., Kriegstein, A.R., 2010. Neurogenic radial glia
717 in the outer subventricular zone of human neocortex. Nature 464, 554–561.
718 doi:10.1038/nature08845
719 Hartfuss, E., Galli, R., Heins, N., Götz, M., 2001. Characterization of CNS precursor
720 subtypes and radial glia. Developmental Biology 229, 15–30.
721 doi:10.1006/dbio.2000.9962
722 Hatakeyama, J., Bessho, Y., Katoh, K., Ookawara, S., Fujioka, M., Guillemot, F.,
723 Kageyama, R., 2004. Hes genes regulate size, shape and histogenesis of the nervous
724 system by control of the timing of neural stem cell differentiation. Development
725 131, 5539–5550. doi:10.1242/dev.01436
726 Hirabayashi, Y., Gotoh, Y., 2010. Epigenetic control of neural precursor cell fate during
727 development. Nat Rev Neurosci 11, 377–388. doi:10.1038/nrn2810
728 Hirabayashi, Y., Suzki, N., Tsuboi, M., Endo, T.A., Toyoda, T., Shinga, J., Koseki, H.,
729 Vidal, M., Gotoh, Y., 2009. Polycomb limits the neurogenic competence of neural
730 precursor cells to promote astrogenic fate transition. Neuron 63, 600–613.
731 doi:10.1016/j.neuron.2009.08.021
732 Huang, D.W., Sherman, B.T., Lempicki, R.A., 2009. Bioinformatics enrichment tools:
733 paths toward the comprehensive functional analysis of large gene lists. Nucleic
734 Acids Research 37, 1–13. doi:10.1093/nar/gkn923
735 Kim, D., Paggi, J.M., Park, C., Bennett, C., Salzberg, S.L., 2019. Graph-based genome
736 alignment and genotyping with HISAT2 and HISAT-genotype. Nat Biotechnol 37,
737 907–915. doi:10.1038/s41587-019-0201-4
738 Kishi, Y., Fujii, Y., Hirabayashi, Y., Gotoh, Y., 2012. HMGA regulates the global
739 chromatin state and neurogenic potential in neocortical precursor cells. Nature
740 Neuroscience 15, 1127–1133. doi:10.1038/nn.3165
741 Kishi, Y., Gotoh, Y., 2018. Regulation of Chromatin Structure During Neural
742 Development. Front Neurosci 12, 874. doi:10.3389/fnins.2018.00874
743 Kornack, D.R., Rakic, P., 1998. Changes in cell-cycle kinetics during the development
744 and evolution of primate neocortex. Proc. Natl. Acad. Sci. U.S.A. 95, 1242–1246.

745 doi:10.1073/pnas.95.3.1242
746 Kriegstein, A., Alvarez-Buylla, A., 2009. The Glial Nature of Embryonic and Adult
747 Neural Stem Cells. Annu. Rev. Neurosci. 32, 149–184.
748 doi:10.1146/annurev.neuro.051508.135600
749 Ku, M., Koche, R.P., Rheinbay, E., Mendenhall, E.M., Endoh, M., Mikkelsen, T.S.,
750 Presser, A., Nusbaum, C., Xie, X., Chi, A.S., Adli, M., Kasif, S., Ptaszek, L.M.,
751 Cowan, C.A., Lander, E.S., Koseki, H., Bernstein, B.E., 2008. Genomewide
752 analysis of PRC1 and PRC2 occupancy identifies two classes of bivalent domains.
753 PLoS Genet 4, e1000242. doi:10.1371/journal.pgen.1000242
754 Lange, C., Turrero Garcia, M., Decimo, I., Bifari, F., Eelen, G., Quaegebeur, A., Boon,
755 R., Zhao, H., Boeckx, B., Chang, J., Wu, C., le Noble, F., Lambrechts, D.,
756 Dewerchin, M., Kuo, C.J., Huttner, W.B., Carmeliet, P., 2016. Relief of hypoxia by
757 angiogenesis promotes neural stem cell differentiation by targeting glycolysis. The
758 EMBO Journal 35, 924–941. doi:10.15252/embj.201592372
759 Langmead, B., Trapnell, C., Pop, M., Salzberg, S.L., 2009. Ultrafast and memory-
760 efficient alignment of short DNA sequences to the human genome. Genome
761 Biology 10, R25–10. doi:10.1186/gb-2009-10-3-r25
762 Lee, Y.S., Dutta, A., 2007. The tumor suppressor microRNA let-7 represses the
763 HMGA2 oncogene. Genes & Development 21, 1025–1030.
764 doi:10.1101/gad.1540407
765 Li, H., Liefke, R., Jiang, J., Kurland, J.V., Tian, W., Deng, P., Zhang, W., He, Q., Patel,
766 D.J., Bulyk, M.L., Shi, Y., Wang, Z., 2017. Polycomb-like proteins link the PRC2
767 complex to CpG islands. Nature 549, 287–291. doi:10.1038/nature23881
768 Li, Z., Gilbert, J.A., Zhang, Y., Zhang, M., Qiu, Q., Ramanujan, K., Shavlakadze, T.,
769 Eash, J.K., Scaramozza, A., Goddeeris, M.M., Kirsch, D.G., Campbell, K.P., Brack,
770 A.S., Glass, D.J., 2012. An HMGA2-IGF2BP2 axis regulates myoblast proliferation
771 and myogenesis. Developmental Cell 23, 1176–1188.
772 doi:10.1016/j.devcel.2012.10.019
773 Liao, Y., Smyth, G.K., Shi, W., 2014. featureCounts: an efficient general purpose
774 program for assigning sequence reads to genomic features. Bioinformatics 30, 923–
775 930. doi:10.1093/bioinformatics/btt656
776 Matsui, A., Yoshida, A.C., Kubota, M., Ogawa, M., Shimogori, T., 2011. Mouse in
777 utero electroporation: controlled spatiotemporal gene transfection. J Vis Exp.

778 doi:10.3791/3024
779 Mayr, C., Hemann, M.T., Bartel, D.P., 2007. Disrupting the pairing between let-7 and
780 Hmga2 enhances oncogenic transformation. Science 315, 1576–1579.
781 doi:10.1126/science.1137999
782 McLone, D.G., Bondareff, W., 1975. Developmental morphology of the subarachnoid
783 space and contiguous structures in the mouse. Am. J. Anat. 142, 273–293.
784 doi:10.1002/aja.1001420302
785 Mikkelsen, T.S., Ku, M., Jaffe, D.B., Issac, B., Lieberman, E., Giannoukos, G.,
786 Alvarez, P., Brockman, W., Kim, T.-K., Koche, R.P., Lee, W., Mendenhall, E.,
787 O'Donovan, A., Presser, A., Russ, C., Xie, X., Meissner, A., Wernig, M., Jaenisch,
788 R., Nusbaum, C., Lander, E.S., Bernstein, B.E., 2007. Genome-wide maps of
789 chromatin state in pluripotent and lineage-committed cells. Nature 448, 553–560.
790 doi:10.1038/nature06008
791 Miyata, T., Kawaguchi, A., Saito, K., Kuramochi, H., Ogawa, M., 2002. Visualization
792 of cell cycling by an improvement in slice culture methods. J. Neurosci. Res. 69,
793 861–868. doi:10.1002/jnr.10335
794 Mohn, F., Weber, M., Rebhan, M., Roloff, T.C., Richter, J., Stadler, M.B., Bibel, M.,
795 Schübeler, D., 2008. Lineage-specific polycomb targets and de novo DNA
796 methylation define restriction and potential of neuronal progenitors. Molecular Cell
797 30, 755–766. doi:10.1016/j.molcel.2008.05.007
798 Morimoto-Suzki, N., Hirabayashi, Y., Tyssowski, K., Shinga, J., Vidal, M., Koseki, H.,
799 Gotoh, Y., 2014. The polycomb component Ring1B regulates the timed termination
800 of subcerebral projection neuron production during mouse neocortical development.
801 Development 141, 4343–4353. doi:10.1242/dev.112276
802 Mukhtar, T., Taylor, V., 2018. Untangling Cortical Complexity During Development. J
803 Exp Neurosci 12, 1179069518759332. doi:10.1177/1179069518759332
804 Nakagawa, T., Wada, Y., Katada, S., Kishi, Y., 2020. Epigenetic regulation for
805 acquiring glial identity by neural stem cells during cortical development. Glia 14,
806 67–14. doi:10.1002/glia.23818
807 Nguyen, H., Kerimoglu, C., Pirouz, M., Pham, L., Kiszka, K.A., Sokpor, G., Sakib,
808 M.S., Rosenbusch, J., Teichmann, U., Seong, R.H., Stoykova, A., Fischer, A.,
809 Staiger, J.F., Tuoc, T., 2018. Epigenetic Regulation by BAF Complexes Limits
810 Neural Stem Cell Proliferation by Suppressing Wnt Signaling in Late Embryonic

811 Development. Stem Cell Reports. doi:10.1016/j.stemcr.2018.04.014
812 Nishino, J., Kim, I., Chada, K., Morrison, S.J., 2008. Hmga2 promotes neural stem cell
813 self-renewal in young but not old mice by reducing p16Ink4a and p19Arf
814 Expression. Cell 135, 227–239. doi:10.1016/j.cell.2008.09.017
815 Noctor, S.C., Flint, A.C., Weissman, T.A., Dammerman, R.S., Kriegstein, A.R., 2001.
816 Neurons derived from radial glial cells establish radial units in neocortex. Nature
817 409, 714–720. doi:10.1038/35055553
818 Nowakowski, T.J., Bhaduri, A., Pollen, A.A., Alvarado, B., Mostajo-Radji, M.A., Di
819 Lullo, E., Haeussler, M., Sandoval-Espinosa, C., Liu, S.J., Velmeshev, D.,
820 Ounadjela, J.R., Shuga, J., Wang, X., Lim, D.A., West, J.A., Leyrat, A.A., Kent,
821 W.J., Kriegstein, A.R., 2017. Spatiotemporal gene expression trajectories reveal
822 developmental hierarchies of the human cortex. Science 358, 1318–1323.
823 doi:10.1126/science.aap8809
824 Otani, T., Marchetto, M.C., Gage, F.H., Simons, B.D., Livesey, F.J., 2016. 2D and 3D
825 Stem Cell Models of Primate Cortical Development Identify Species-Specific
826 Differences in Progenitor Behavior Contributing to Brain Size. Cell Stem Cell 18,
827 467–480. doi:10.1016/j.stem.2016.03.003
828 Pereira, J.D., Sansom, S.N., Smith, J., Dobenecker, M.-W., Tarakhovsky, A., Livesey,
829 F.J., 2010. Ezh2, the histone methyltransferase of PRC2, regulates the balance
830 between self-renewal and differentiation in the cerebral cortex. Proceedings of the
831 National Academy of Sciences 107, 15957–15962. doi:10.1073/pnas.1002530107
832 Qian, X., Goderie, S.K., Shen, Q., Stern, J.H., Temple, S., 1998. Intrinsic programs of
833 patterned cell lineages in isolated vertebrate CNS ventricular zone cells.
834 Development 125, 3143–3152.
835 Quah, B.J.C., Parish, C.R., 2010. The use of carboxyfluorescein diacetate succinimidyl
836 ester (CFSE) to monitor lymphocyte proliferation. J Vis Exp. doi:10.3791/2259
837 Quinlan, A.R., Hall, I.M., 2010. BEDTools: a flexible suite of utilities for comparing
838 genomic features. Bioinformatics 26, 841–842. doi:10.1093/bioinformatics/btq033
839 Rakic, P., 2009. Evolution of the neocortex: a perspective from developmental biology.
840 Nat Rev Neurosci 10, 724–735. doi:10.1038/nrn2719
841 Rakic, P., 1995. A small step for the cell, a giant leap for mankind: a hypothesis of
842 neocortical expansion during evolution. Trends in Neurosciences 18, 383–388.
843 doi:10.1016/0166-2236(95)93934-p

844 Rakic, P., 1972. Mode of cell migration to the superficial layers of fetal monkey
845 neocortex. J. Comp. Neurol. 145, 61–83. doi:10.1002/cne.901450105
846 Sahara, S., O'Leary, D.D.M., 2009. Fgf10 regulates transition period of cortical stem
847 cell differentiation to radial glia controlling generation of neurons and basal
848 progenitors. Neuron 63, 48–62. doi:10.1016/j.neuron.2009.06.006
849 Sakai, H., Fujii, Y., Kuwayama, N., Kawaji, K., Gotoh, Y., Kishi, Y., 2019. Plag1
850 regulates neuronal gene expression and neuronal differentiation of neocortical
851 neural progenitor cells. Genes to Cells 24, 650–666. doi:10.1111/gtc.12718
852 Sanosaka, T., Namihira, M., Asano, H., KOHYAMA, J., Aisaki, K., Igarashi, K.,
853 Kanno, J., Nakashima, K., 2008. Identification of genes that restrict astrocyte
854 differentiation of midgestational neural precursor cells. Neuroscience 155, 780–788.
855 doi:10.1016/j.neuroscience.2008.06.039
856 Sasagawa, Y., Nikaido, I., Hayashi, T., Danno, H., Uno, K.D., Imai, T., Ueda, H.R.,
857 2013. Quartz-Seq: a highly reproducible and sensitive single-cell RNA sequencing
858 method, reveals non-genetic gene-expression heterogeneity. Genome Biology 14,
859 R31. doi:10.1186/gb-2013-14-4-r31
860 Shen, Q., Wang, Y., Dimos, J.T., Fasano, C.A., Phoenix, T.N., Lemischka, I.R.,
861 Ivanova, N.B., Stifani, S., Morrisey, E.E., Temple, S., 2006. The timing of cortical
862 neurogenesis is encoded within lineages of individual progenitor cells. Nature
863 Neuroscience 9, 743–751. doi:10.1038/nn1694
864 Shi, Y., Kirwan, P., Smith, J., Robinson, H.P.C., Livesey, F.J., 2012. Human cerebral
865 cortex development from pluripotent stem cells to functional excitatory synapses.
866 Nature Neuroscience 15, 477–86– S1. doi:10.1038/nn.3041
867 Siegenthaler, J.A., Ashique, A.M., Zarbalis, K., Patterson, K.P., Hecht, J.H., Kane,
868 M.A., Folias, A.E., Choe, Y., May, S.R., Kume, T., Napoli, J.L., Peterson, A.S.,
869 Pleasure, S.J., 2009. Retinoic acid from the meninges regulates cortical neuron
870 generation. Cell 139, 597–609. doi:10.1016/j.cell.2009.10.004
871 Subramanian, A., Tamayo, P., Mootha, V.K., Mukherjee, S., Ebert, B.L., Gillette, M.A.,
872 Paulovich, A., Pomeroy, S.L., Golub, T.R., Lander, E.S., Mesirov, J.P., 2005. Gene
873 set enrichment analysis: A knowledge-based approach for interpreting genome-
874 wide expression profiles. Proc. Natl. Acad. Sci. U.S.A. 102, 15545–15550.
875 doi:10.1073/pnas.0506580102
876 Sun, T., Hevner, R.F., 2014. Growth and folding of the mammalian cerebral cortex:

877 from molecules to malformations. Nat Rev Neurosci 15, 217–232.
878 doi:10.1038/nrn3707
879 Tabata, H., Nakajima, K., 2001. Efficient in utero gene transfer system to the
880 developing mouse brain using electroporation: visualization of neuronal migration
881 in the developing cortex. Neuroscience 103, 865–872. doi:10.1016/s0306-
882 4522(01)00016-1
883 Telley, L., Govindan, S., Prados, J., Stévant, I., Nef, S., Dermitzakis, E., Dayer, A.,
884 Jabaudon, D., 2016. Sequential transcriptional waves direct the differentiation of
885 newborn neurons in the mouse neocortex. Science 351, 1443–1446.
886 doi:10.1126/science.aad8361
887 Tessari, M.A., Gostissa, M., Altamura, S., Sgarra, R., Rustighi, A., Salvagno, C.,
888 Caretti, G., Imbriano, C., Mantovani, R., Del Sal, G., Giancotti, V., Manfioletti, G.,
889 2003. Transcriptional activation of the cyclin A gene by the architectural
890 transcription factor HMGA2. Molecular and Cellular Biology 23, 9104–9116.
891 Tsuboi, M., Hirabayashi, Y., Gotoh, Y., 2019. Diverse gene regulatory mechanisms
892 mediated by Polycomb group proteins during neural development. Current Opinion
893 in Neurobiology 59, 164–173. doi:10.1016/j.conb.2019.07.003
894 Tsuboi, M., Kishi, Y., Yokozeki, W., Koseki, H., Hirabayashi, Y., Gotoh, Y., 2018.
895 Ubiquitination-Independent Repression of PRC1 Targets during Neuronal Fate
896 Restriction in the Developing Mouse Neocortex. Developmental Cell 47, 758–
897 772.e5. doi:10.1016/j.devcel.2018.11.018
898 Vignali, R., Marracci, S., 2020. HMGA Genes and Proteins in Development and
899 Evolution. IJMS 21, 654–39. doi:10.3390/ijms21020654
900 Winter, N., Nimzyk, R., Bösche, C., Meyer, A., Bullerdiek, J., 2011. Chromatin
901 immunoprecipitation to analyze DNA binding sites of HMGA2. PLoS ONE 6,
902 e18837. doi:10.1371/journal.pone.0018837
903 Yoon, K., Nery, S., Rutlin, M.L., Radtke, F., Fishell, G., Gaiano, N., 2004. Fibroblast
904 growth factor receptor signaling promotes radial glial identity and interacts with
905 Notch1 signaling in telencephalic progenitors. Journal of Neuroscience 24, 9497–
906 9506. doi:10.1523/JNEUROSCI.0993-04.2004
907 Yoon, K.-J., Ringeling, F.R., Vissers, C., Jacob, F., Pokrass, M., Jimenez-Cyrus, D., Su,
908 Y., Kim, N.-S., Zhu, Y., Zheng, L., Kim, S., Wang, X., Doré, L.C., Jin, P., Regot,
909 S., Zhuang, X., Canzar, S., He, C., Ming, G.-L., Song, H., 2017. Temporal Control

910 of Mammalian Cortical Neurogenesis by m(6)A Methylation. Cell 171, 877–
911 889.e17. doi:10.1016/j.cell.2017.09.003
912 Zahr, S.K., Yang, G., Kazan, H., Borrett, M.J., Yuzwa, S.A., Voronova, A., Kaplan,
913 D.R., Miller, F.D., 2018. A Translational Repression Complex in Developing
914 Mammalian Neural Stem Cells that Regulates Neuronal Specification. Neuron 97,
915 520–537.e6. doi:10.1016/j.neuron.2017.12.045
916 Zhang, X., Chen, M.H., Wu, X., Kodani, A., Fan, J., Doan, R., Ozawa, M., Ma, J.,
917 Yoshida, N., Reiter, J.F., Black, D.L., Kharchenko, P.V., Sharp, P.A., Walsh, C.A.,
918 2016. Cell-Type-Specific Alternative Splicing Governs Cell Fate in the Developing
919 Cerebral Cortex. Cell 166, 1147–1162.e15. doi:10.1016/j.cell.2016.07.025
920
921

922 **Figure Legends**

923

924 **Figure 1. In utero injection of mouse embryos before neural tube closure.** (**a** and **b**)
925 The uterine horn of an anesthetized pregnant mouse was exposed at E7.0 or E8.0. (**c** and
926 **d**) The uterus was pinched between an optical fiber and finger (**c**) for injection via a
927 sharpened glass capillary of a solution colored with a dye (FastGreen) and containing
928 either CFSE, a retrovirus, or a plasmid (**d**).

929

930 **Figure 2. In utero gene introduction by retroviral infection in embryos before**
931 **neural tube closure.** (**a**) Mouse embryos in the same uterus were injected or not with a
932 retrovirus encoding GFP together with an shRNA targeted to luciferase mRNA at E8.0.
933 The embryos were dissected out from the uterus at E11.0, fixed, and examined for GFP
934 fluorescence with a fluorescence stereo microscope. The posterior half of the control
935 embryo was excised for the purpose of identification. Scale bars, 1 mm. (**b**) An embryo
936 at E7.0 was injected as in (**a**) and examined for GFP fluorescence at E11.0. Scale bar, 1
937 mm. (**c**) Survival rate and labeling rate for embryos injected as in (**a**) and (**b**). (**d**) Flow
938 cytometric analysis of the efficiency of gene introduction. Neocortical cells dissociated
939 from E12.0 embryos that had been injected with a retrovirus for GFP at E8.0 were
940 subjected to flow cytometric analysis of GFP expression. (**e**) A sagittal section of an
941 E10.0 embryo injected at E8.0 as in (**a**) was subjected to immunohistofluorescence
942 staining with antibodies to GFP. Nuclei were counterstained with Hoechst 33342.
943 Representative infected tissues are indicated. Scale bar, 1 mm. (**f**, **g**) Higher
944 magnification images of the bronchus (**f**) and spinal cord (**g**) in the section shown in (**e**).
945 Scale bars, 100 μm.

946

947 **Figure 3. Hierarchical clustering of differentially expressed genes in NPCs at early**
948 **developmental stages.** (**a**) CD133^{high} cells were isolated as NPCs from the
949 telencephalon at E8.0 and E9.0 and from the neocortex at E10.0, E11.0, and E12.0 by
950 FACS and were subjected to RNA-seq analysis. (**b**–**f**) Differentially expressed genes in
951 NPCs at the various developmental stages isolated as in (**a**) were categorized into five
952 clusters (clusters 1–5) on the basis of the pattern of expression changes with the use of
953 hierarchical clustering analysis. The expression levels of the genes in each gene cluster
954 are shown as box plots, with the boxes representing the median and upper and lower

955 quartiles and the whiskers indicating the range (left). Enriched GO terms and their *p*
956 values determined by functional annotation of each gene cluster with DAVID software
957 are also shown (right). RPKM, reads per kilobase of mRNA per million total reads. (**g**)
958 The five genes expressed at the highest levels in cluster 5 at E10.0. (**h**) NPCs isolated as
959 in (**a**) from embryos at E9.0, E10.0, E11.0, and E12.0 were subjected to RT-qPCR
960 analysis of *Hmga2* mRNA. Data were normalized by *Actb* mRNA abundance and are
961 means + SEM from five independent experiments. $*p < 0.05$, $**p < 0.01$ (one-way
962 ANOVA followed by the Bonferroni-Holm multiple-comparison test).
963
964 **Figure 4. Hmga2 promotes the onset of neurogenesis in the mouse neocortex.** (**a**)
965 Mouse embryos at E8.0 were subjected to in utero infection with retroviruses encoding
966 GFP and either control or Hmga2 shRNAs, and the brain was isolated from the embryos
967 at E10.0 or E11.0 for isolation of $CD133^{high}$, GFP^{+} NPCs by FACS. (**b**) NPCs isolated
968 from control and Hmga2–knockdown (KD) embryos as in (**a**) were subjected to RT-
969 qPCR analysis of *Hmga2* mRNA. Data are expressed relative to the corresponding
970 control value and are means + SEM from five independent experiments. $*p < 0.05$, $**p$
971 < 0.01 versus corresponding control value (two-tailed Student's paired *t* test). (**c**–**g**) The
972 brain of embryos treated as in (**a**) was subjected to immunohistofluorescence analysis
973 with antibodies to GFP and to Hmga2 at E10.0 (**c**), with those to GFP and toTbr2 at
974 E11.0 (**d**), and with those to GFP and to Sox2 at E11.0 (**f**). Nuclei were counterstained
975 with Hoechst 33342. Scale bars, 20 μm (**c**) or 50 μm (**d** and **f**). Arrowheads indicate
976 GFP^{+} cells (**c**). The percentages of $Tbr2^{+}$ cells at E10.0 or E11.0 (**e**) or of $Sox2^{+}$ cells at
977 E11.0 (**g**) among GFP^{+} cells were also determined. Data are means + SEM from six
978 (Tbr2) or three (Sox2) independent experiments (total of 12 control and nine Hmga2-
979 knockdown embryos for Tbr2, and eight control and seven Hmga2-knockdown embryos
980 for Sox2). $*p < 0.05$ versus corresponding control value (two-tailed Welch's *t* test).
981
982 **Figure 5. Hmga2 promotes the change in transcriptional profile of NPCs at the E-**
983 **to-N transition.** (**a**) Embryos were subjected to in utero infection with retroviruses
984 encoding GFP and either control or Hmga2 shRNAs at E8.0, and the brain was isolated
985 at E10.0 or E11.0 for isolation of GFP^{+}, $CD133^{high}$ NPCs by FACS and subsequent RNA
986 (Quartz)-seq analysis. Three or four independent experiments were performed with cells
987 isolated at E10.0 or E11.0, respectively. (**b**) Expression levels (RPKM) of *Hmga2* and

988 *Igf2bp2* in Hmga2–knockdown (KD) and control NPCs determined as in (**a**). Data are
989 means + SEM and are expressed relative to the corresponding control value. *$p < 0.05$,
990 **$p < 0.01$ versus corresponding control value (two-tailed Student's paired *t* test). (**c**)
991 NPCs isolated at E10.0 as in (**a**) were subjected to GSEA for signature genes of the
992 expansion phase (those in cluster 2 with an RPKM of ≥50 at E9.0) (Figure 3c). The
993 family-wise error rate (FWER) *p* value and false discovery rate (FDR) *q* value are
994 shown.
995
996 **Figure 6. Hmga2 promotes the expression of PcG target genes in NPCs.** (**a**) Cells
997 isolated from the mouse neocortex at E11.0 were subjected to ChIP-seq for Hmga2
998 (four independent experiments). CD133^{high} cells sorted by FACS were used for the
999 H3K27me3 analysis (three independent experiments). The genome-wide correlation
1000 heat map based on the Jaccard index for determined peaks in the samples is shown. (**b**)
1001 The Quartz-seq data for NPCs at E11.0 in Figure 5 were subjected to GSEA of PcG
1002 target genes previously identified by Ring1B knockout (KO) in an NPC culture
1003 (Hirabayashi et al., 2009). The FWER *p* value and FDR *q* value are shown. (**c**) The
1004 Quartz-seq data for NPCs at E11.0 in Figure 5 were subjected to GSEA of PcG target
1005 genes that we identified by RNA-seq analysis of NPCs isolated by FACS at E18 from
1006 the neocortex of *Ring1a*$^{-/-}$;*Ring1b*$^{flox/flox}$;*Rosa-CreERT2*$^{-/-\text{ or }+/-}$ mouse embryos that had
1007 been treated with tamoxifen at E15 (see Materials and Methods). The FWER *p* value
1008 and FDR *q* value are shown. (**d**) GO terms and their *p* values determined by functional
1009 annotation of core enrichment genes in the GSEA analyses shown in (**b**) and (**c**) with the
1010 use of DAVID software.
1011

1012 **Supplemental Figure Legends**

1013 **Figure S1. In utero injection of CFSE into mouse embryos before neural tube**
1014 **closure.** (**a**) Embryos at E7.0 (left) or E8.0 (right) were injected with CFSE, dissected
1015 out from the uterus at E9.0 or E11.0, respectively, and fixed for visualization of CFSE
1016 fluorescence with a fluorescence stereo microscope. Scale bars, 0.5 mm (left) or 1 mm
1017 (right). (**b**) Survival rate and labeling rate for in utero introduction of CFSE into mouse
1018 embryos as in (**a**).

1019

1020 **Figure S2. In utero electroporation of embryos before neural tube closure.** (**a**)
1021 Embryos at E7.0 (left) or E8.0 (right) were injected with a plasmid for mCherry and
1022 subjected to in utero electroporation. They were dissected out from the uterus at E9.0 or
1023 E10.0, respectively, fixed, and examined for mCherry fluorescence with a fluorescence
1024 stereo microscope. Scale bars, 0.5 mm (left) or 1 mm (right). (**b**) Survival rate and
1025 labeling rate for in utero electroporation of embryos as in (**a**).

1026

Fig. 1

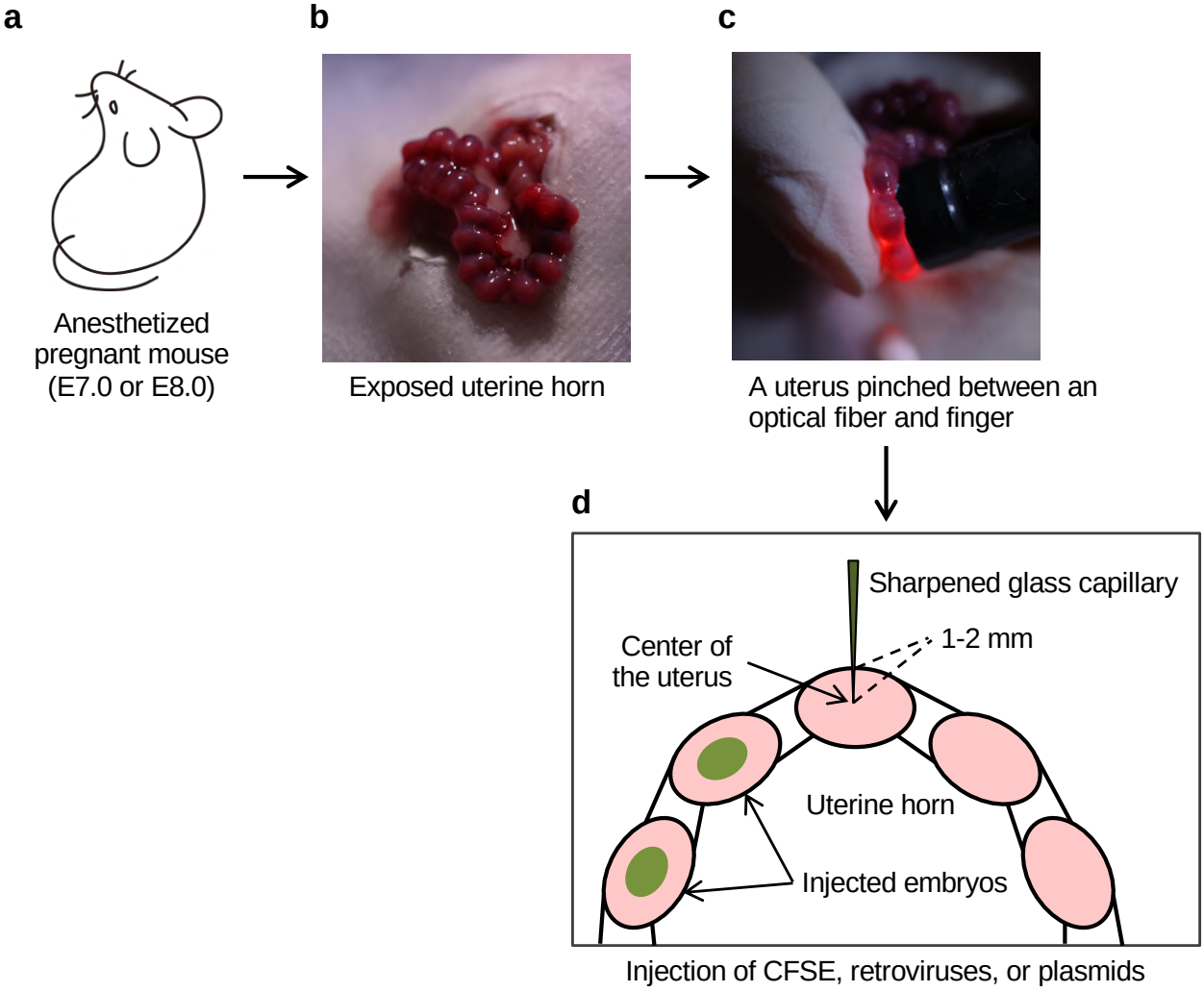
a
b
c
Anesthetized pregnant mouse (E7.0 or E8.0)
Exposed uterine horn
A uterus pinched between an optical fiber and finger
d
Sharpened glass capillary
1-2 mm
Center of the uterus
Uterine horn
Injected embryos
Injection of CFSE, retroviruses, or plasmids

Fig. 2

a

E8.0 injection → E11.0

Control (no injection) | GFP-expressing virus

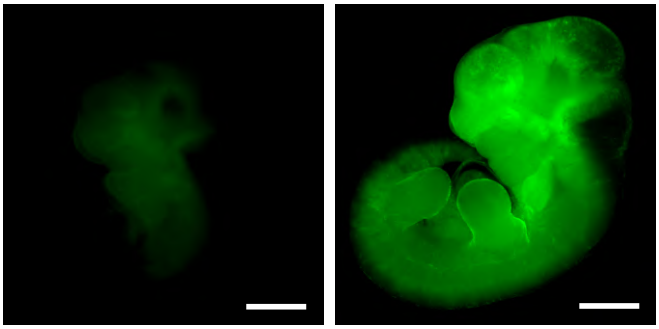

b

E7.0 injection → E11.0

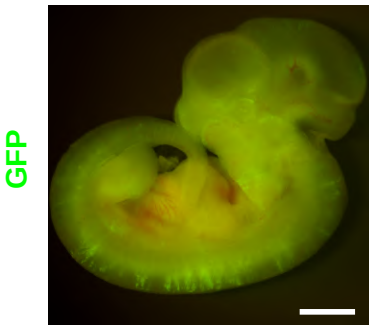

c

	Injected embryos	Survival rate (% of injected)	GFP-positive (% of injected)
E7.0 injection → E9.0	28	27 (96%)	2 (7%)
E8.0 injection → E10.0	19	17 (89%)	14 (74%)

d

E8.0 injection → E12.0

Control (no injection)

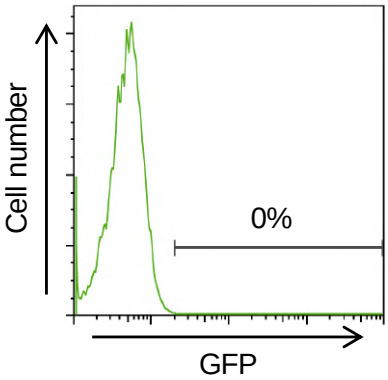

GFP-expressing virus

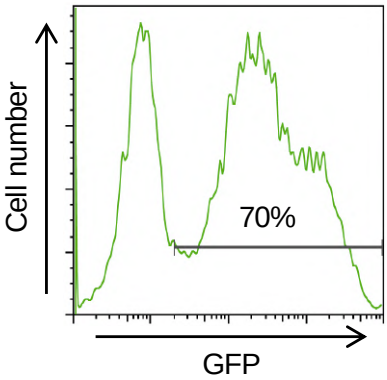

e

E8.0 injection → E10.0

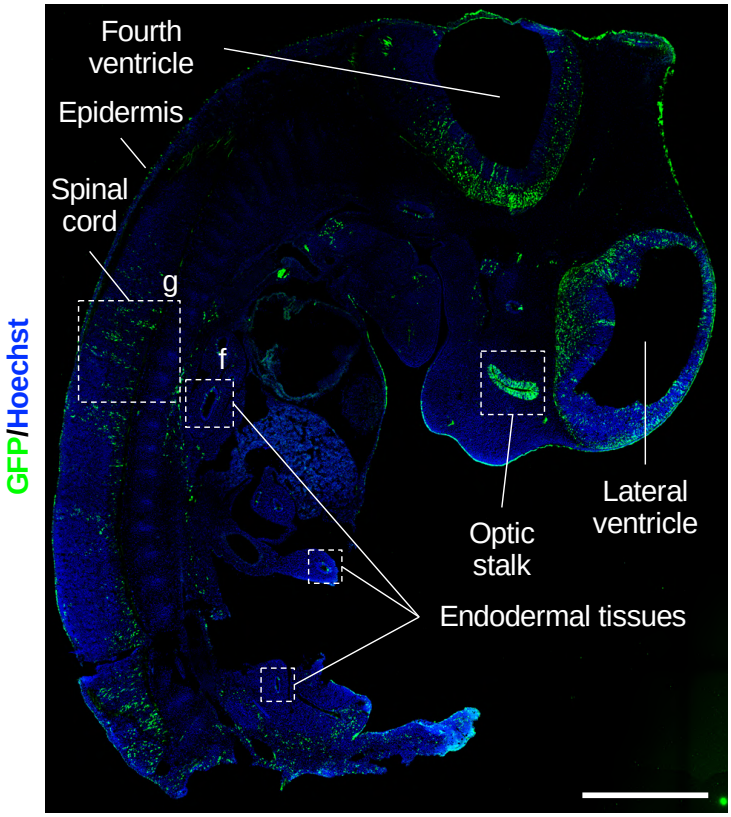

f

Bronchus

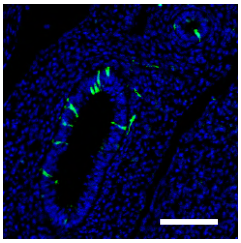

g

Spinal cord

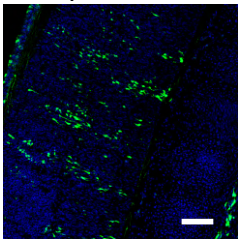

Fig. 3

a

E8.0 whole brain
E9.0 whole brain
E10.0 neocortex
E11.0 neocortex
E12.0 neocortex

→ FACS (CD133^{high}), RNA-seq

b

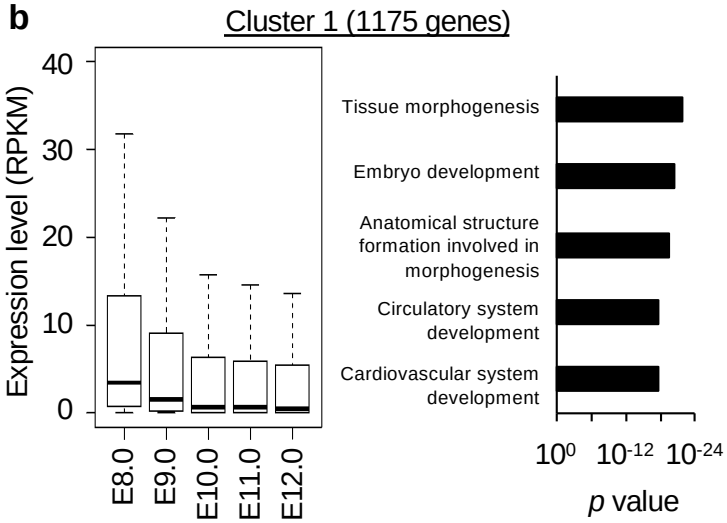

c

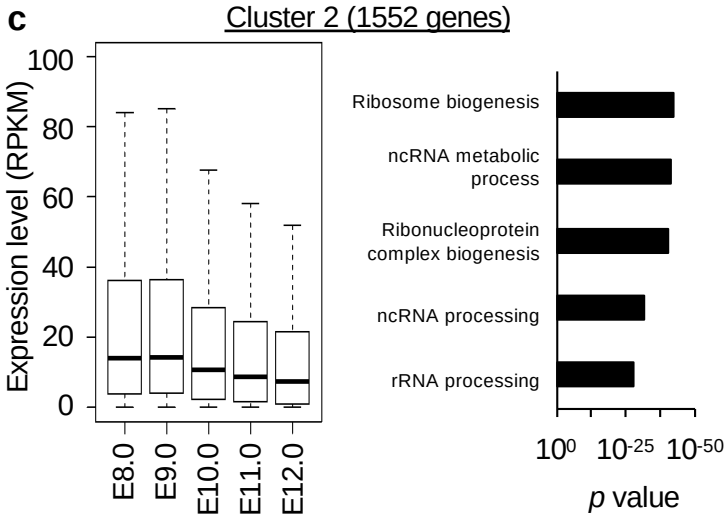

d

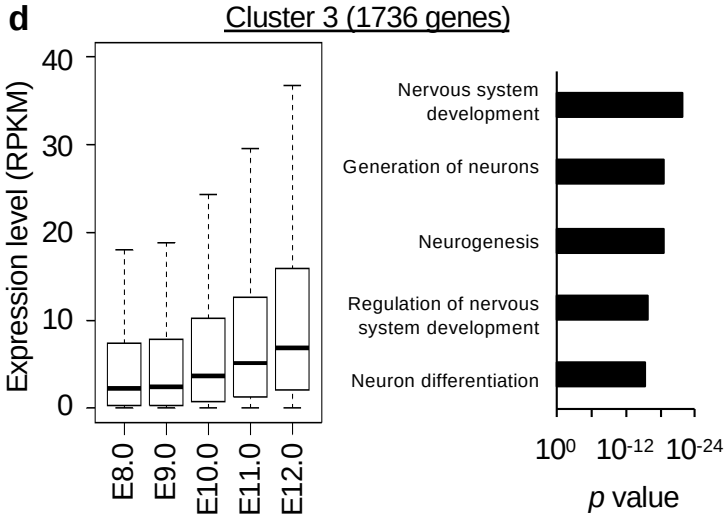

e

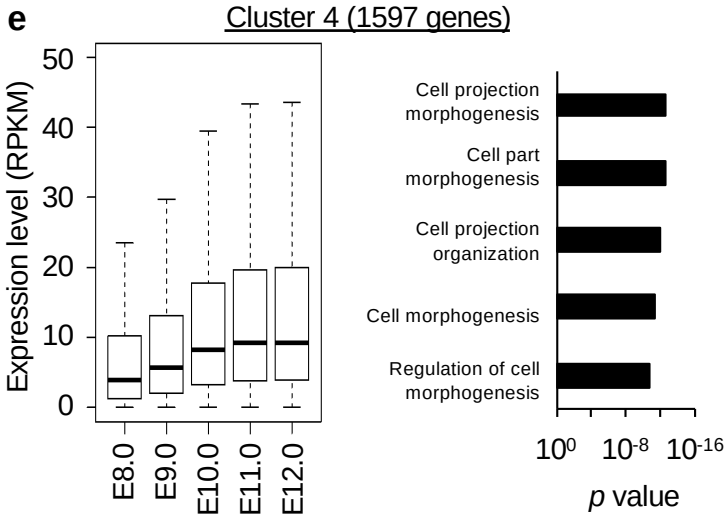

f

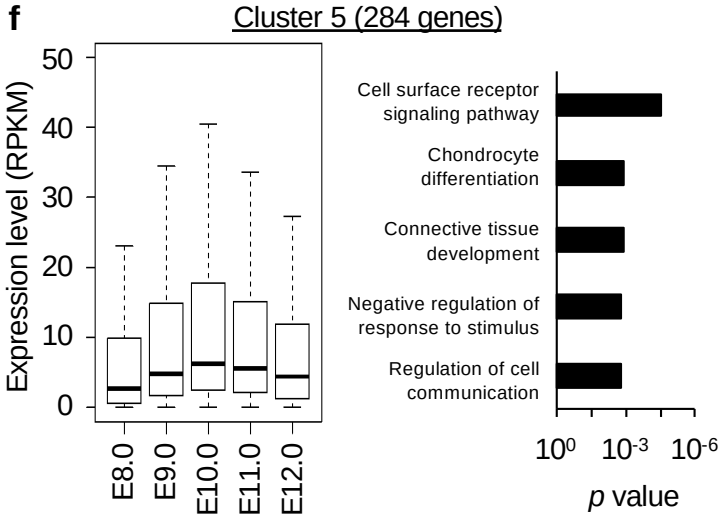

g

Gene symbol	Expression level (RPKM)
Atp5a1	339
Hmga2	279
Lrrn1	217
Calm3	129
Ccnd1	127

h

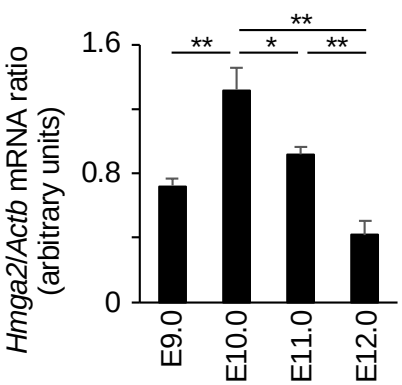

Fig. 4

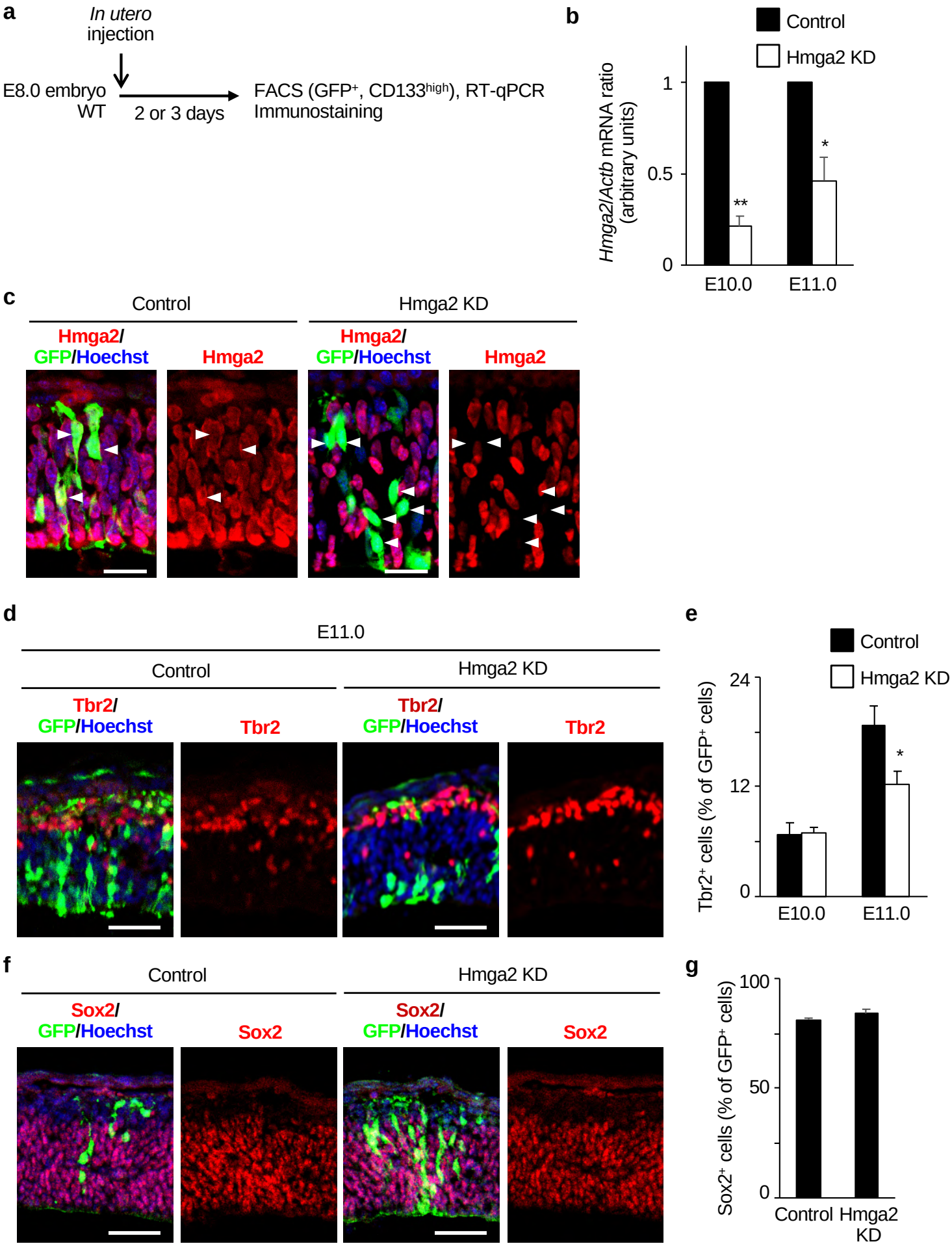
a
In utero injection
E8.0 embryo WT
2 or 3 days
FACS (GFP+, CD133high), RT-qPCR
Immunostaining
b
Control
Hmga2 KD
Hmga2/Actb mRNA ratio (arbitrary units)
1
0.5
0
**
*
E10.0
E11.0
c
Control
Hmga2 KD
Hmga2/ GFP/Hoechst
Hmga2
d
E11.0
Control
Hmga2 KD
Tbr2/ GFP/Hoechst
Tbr2
e
Control
Hmga2 KD
Tbr2+ cells (% of GFP+ cells)
24
12
0
*
E10.0
E11.0
f
Control
Hmga2 KD
Sox2/ GFP/Hoechst
Sox2
g
Sox2+ cells (% of GFP+ cells)
100
50
0
Control
Hmga2 KD

Fig. 5

a

In utero
injection
E8.0 embryo
WT
2 or 3 days
FACS (GFP+, CD133high),
RNA-seq

b

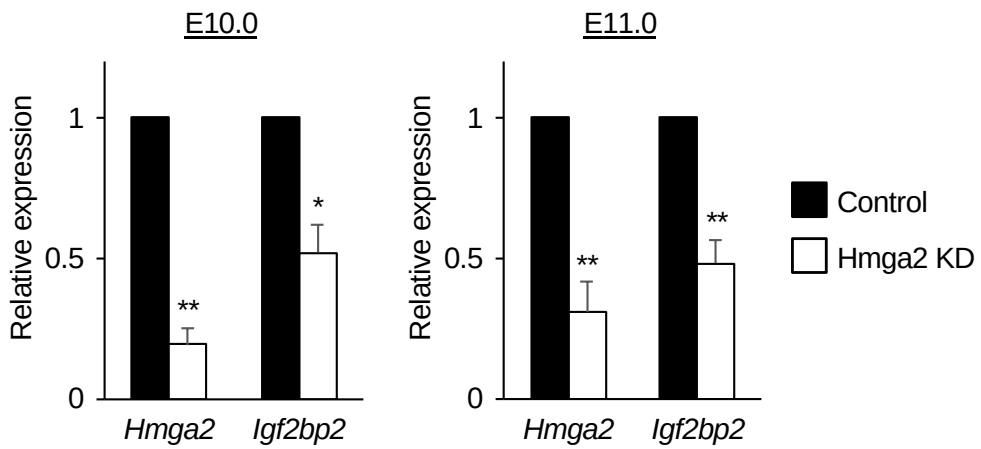
E10.0
E11.0
Relative expression
1
0.5
0
**
*
Hmga2
Igf2bp2
Control
Hmga2 KD

c

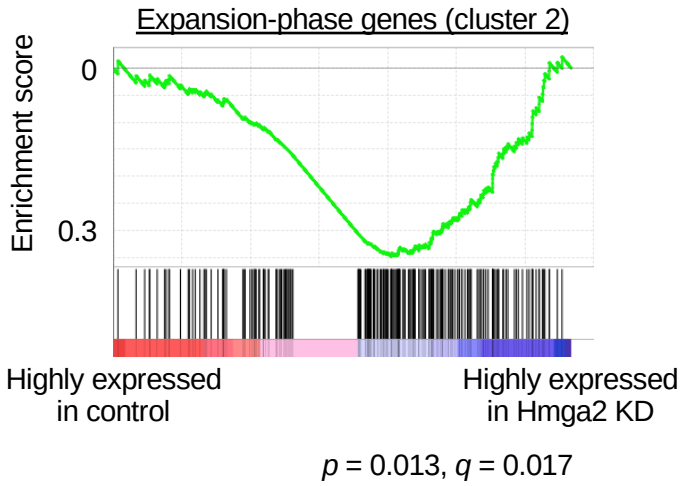
Expansion-phase genes (cluster 2)
Enrichment score
0
0.3
Highly expressed
in control
Highly expressed
in Hmga2 KD
p = 0.013, q = 0.017

Fig. 6

a

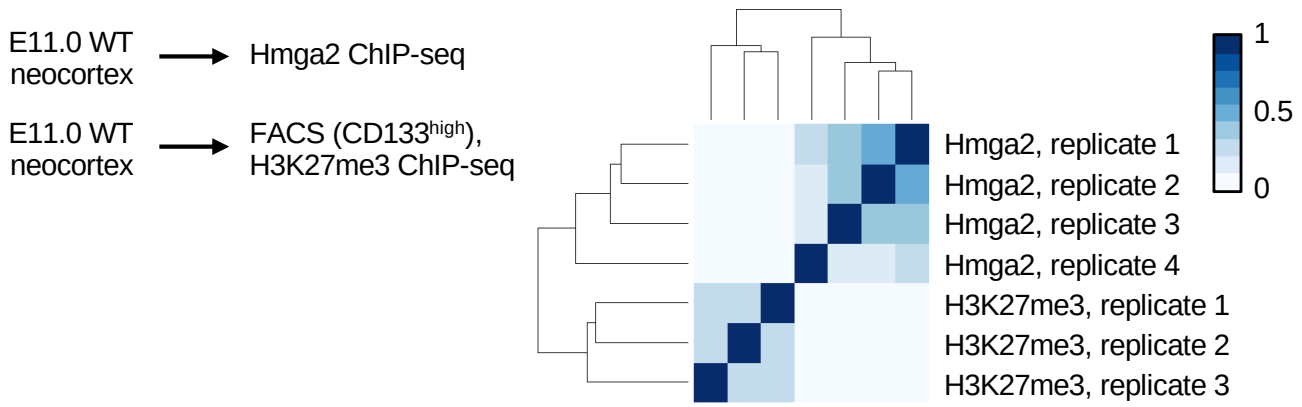
E11.0 WT neocortex
Hmga2 ChIP-seq
E11.0 WT neocortex
FACS (CD133high), H3K27me3 ChIP-seq
Hmga2, replicate 1
Hmga2, replicate 2
Hmga2, replicate 3
Hmga2, replicate 4
H3K27me3, replicate 1
H3K27me3, replicate 2
H3K27me3, replicate 3
1
0.5
0

b

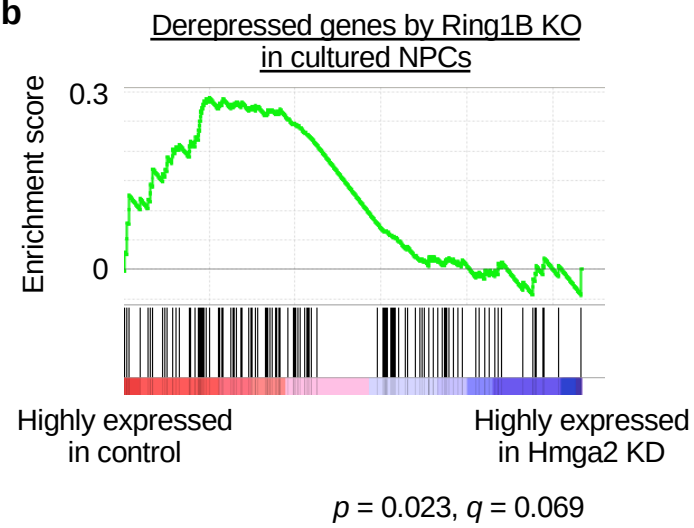
Derepressed genes by Ring1B KO in cultured NPCs
Enrichment score
0.3
0
Highly expressed in control
Highly expressed in Hmga2 KD
p = 0.023, q = 0.069

c

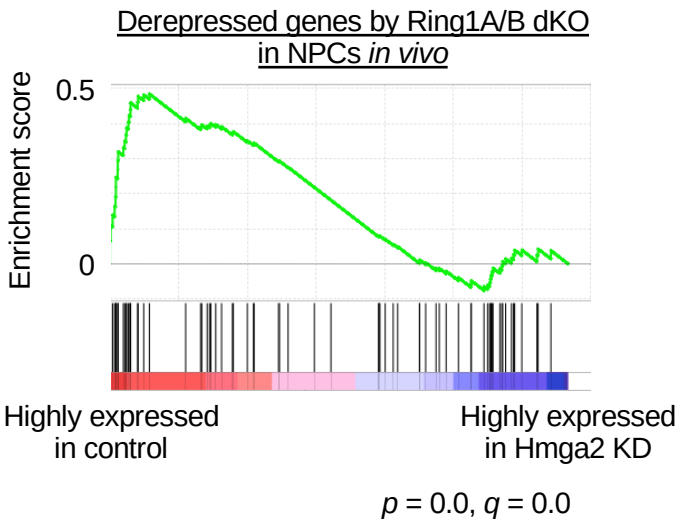
Derepressed genes by Ring1A/B dKO in NPCs in vivo
Enrichment score
0.5
0
Highly expressed in control
Highly expressed in Hmga2 KD
p = 0.0, q = 0.0

d

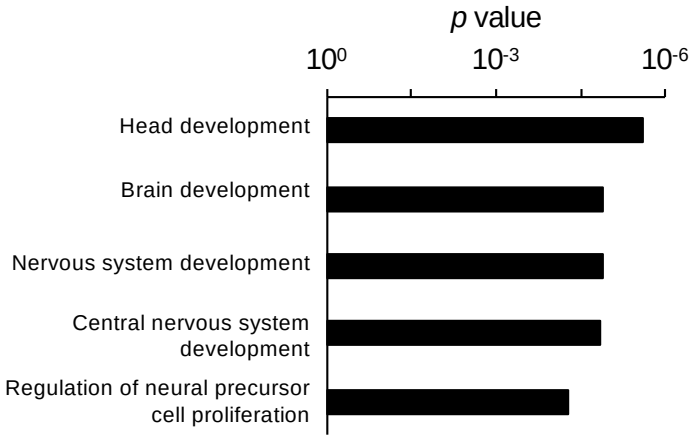
Core enrichment genes in Ring1 KO cells
p value
10^0
10^-3
10^-6
Head development
Brain development
Nervous system development
Central nervous system development
Regulation of neural precursor cell proliferation

Fig. S1

a

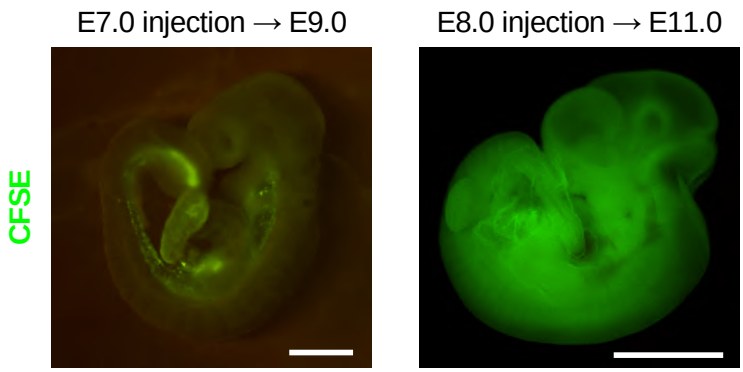

b

	Injected embryos	Survival rate (% of injected)	CFSE-positive (% of injected)
E7.0 injection → E9.0	28	25 (89%)	18 (64%)
E8.0 injection → E10.0	30	24 (80%)	23 (77%)

Fig. S2

a

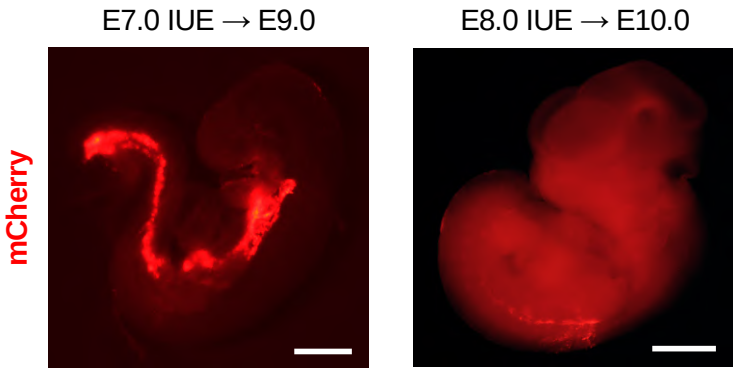

b

	Injected embryos	Survival rate (% of injected)	mCherry-positive (% of injected)
E7.0 injection → E9.0	36	26 (72%)	7 (19%)
E8.0 injection → E10.0	20	11 (55%)	8 (40%)